Thesis for the Degree of Doctor of Philosophy

Longer Wavelength GaAs-Based VCSELs for Extended-Reach Optical Interconnects

Ewa Simpanen

Photonics Laboratory
Department of Microtechnology and Nanoscience (MC2)
Chalmers University of Technology
Göteborg, Sweden 2020

Longer Wavelength GaAs-Based VCSELs for Extended-Reach Optical Interconnects

Ewa Simpanen

ISBN 978-91-7905-242-3

Doktorsavhandlingar vid Chalmers Tekniska Högskola
Ny serie nr 4709
ISSN 0346-718X

Photonics Laboratory
Department of Microtechnology and Nanoscience (MC2)
Chalmers University of Technology
SE-412 96 Göteborg
Sweden
Telephone: +46 (0)31 772 1000

Cover: The image shows a fabricated set of 1060 nm VCSELs on chip.

Printed by Chalmers reproservice, Chalmers University of Technology
Göteborg, Sweden 2020

Longer Wavelength GaAs-Based VCSELs for Extended-Reach Optical Interconnects

Ewa Simpanen

Photonics Laboratory
Department of Microtechnology and Nanoscience (MC2)
Chalmers University of Technology

Abstract

Data centers of today are increasing in size and are built to accommodate strong traffic demands while providing sustainably by having clients sharing resources under one roof. Their massive scale puts pressure on the server network topology and has incited a need for data transmission links that are energy efficient and capable of operation at high bit rates with reach up to a few kilometers. Optical interconnects (OIs) offer large bandwidth and low attenuation at long distances, and are therefore suitable for this task. The most commonly used OIs, with 850 nm GaAs-based vertical-cavity surface-emitting lasers (VCSELs) and multi-mode fiber (MMF), have a 25 Gb/s reach that is limited to a few hundred meters. However, the fiber chromatic dispersion and attenuation that limit the OI reach can be reduced significantly by increasing the wavelength of this very same technology. The upper limit of the GaAs-based VCSEL technology, with strained InGaAs quantum wells (QWs), is about 1100 nm.

With further improved OI performance, new hyperscale data center topologies can be realized and explored. This will lead to a larger number of possible solutions in traffic engineering as well as for power management. 1060 nm VCSELs could soon open up for lane rates of 100+ Gb/s over distances up to 2 km and help reach the Tb/s link speed aim of data center OI standards, in which capacity is built up mainly by employing multiple parallel lanes, increasing symbol rate by going from binary to four-level pulse amplitude modulation (PAM-4), and optimizing with electrical mitigation techniques such as digital signal processing.

In this work we show that 1060 nm GaAs VCSELs are suitable light sources for long-reach OIs by first demonstrating their overall stable performance and capability of error-free data transmission up to 50 Gb/s back-to-back and 25 Gb/s over 1 km of MMF. With PAM-4, we show 100 Gb/s error-free capability over 100 m of MMF, suitable for wavelength division multiplexed OIs that can transmit data at several wavelengths from 850 to 1060 nm over the same fiber channel. We also assemble single-mode 1060 nm VCSEL and single-mode fiber links and demonstrate 50 Gb/s error-free transmission over 1 km using pre-emphasis and 40 Gb/s over 2 km without the use of any electrical mitigation techniques. These results stem from careful VCSEL design, including strained InGaAs QWs with GaAsP barriers, doped AlGaAs distributed Bragg reflectors, a short optical cavity and multiple oxide layers. In addition, we show that the fabrication of such a device poses no increase in complexity and can be realized using standard processing techniques.

Keywords: vertical-cavity surface-emitting laser, optical interconnect, chromatic dispersion, attenuation, reach, high-speed modulation, single-mode, multi-mode

List of Papers

This thesis is based on the following appended papers:

[A] **E. Simpanen**, J. S. Gustavsson, E. Haglund, E. P. Haglund, A. Larsson, W. V. Sorin, S. Mathai, and M. R. Tan, "1060 nm single-mode vertical-cavity surface-emitting laser operating at 50 Gbit/s data rate," *Electronics Letters*, vol. 53, no. 13, pp. 869-871, June 2017. (Highlighted)

[B] A. Larsson, **E. Simpanen**, J. S. Gustavsson, E. Haglund, E. P. Haglund, T. Lengyel, P. A. Andrekson, W. V. Sorin, S. Mathai, M. R. Tan, and S. R. Bickham, "1060 nm VCSELs for long-reach optical interconnects," *Optical Fiber Technol.*, vol. 44, pp. 36-42, August 2018. (Invited)

[C] **E. Simpanen**, J. S. Gustavsson, A. Larsson, M. Karlsson, W. V. Sorin, S. Mathai, M. R. Tan, and S. R. Bickham, "1060 nm single-mode VCSEL and single-mode fiber links for long-reach optical interconnects," *IEEE J. Lightwave Technol.*, vol. 37, no. 13, pp. 2963-2969, July 2019.

[D] **E. Simpanen**, J. S. Gustavsson, P. Debernardi, W. V. Sorin, S. Mathai, M. R. Tan, and A. Larsson, "Noise properties of single-mode VCSELs: Dependence on current confinement and optical loss," submitted to *IEEE J. Quantum Electron.*, January 2020. (Manuscript)

[E] T. Lengyel, **E. Simpanen**, J. S. Gustavsson, A. Larsson, M. Karlsson, P. A. Andrekson, W. V. Sorin, S. Mathai, M. R. Tan, and S. R. Bickham, "Pre-emphasis enabled 50 Gbit/s transmission over 1000 m SMF using a 1060 nm single-mode VCSEL," *Electronics Letters*, vol. 54, no. 20, pp. 1186-1187, October 2018.

[F] J. Lavrencik, **E. Simpanen**, S. Varughese, A. Melgar, V. A. Thomas, J. S. Gustavsson, W. V. Sorin, S. Mathai, M. R. Tan, A. Larsson, and S. E. Ralph, "Error-free 100Gbps PAM-4 transmission over 100m OM5 MMF using 1060nm VCSELs," *Optical Fiber Communications Conference and Exhibition (OFC)*, San Diego, CA, USA, paper M1F.3, March 2019.

Related publications and conference contributions by the author:

[G] S. R. Bickham, P. Tandon, S. K. Mishra, M.-J. Li, **E. Simpanen**, T. Lengyel, J. S. Gustavsson, and A. Larsson, "Low cutoff G.657-compatible fibers for data center interconnects operating in the 1064 and 1310 nm windows," presented at *SPIE Photonics West*, February 2020. To be published in *Proc. SPIE*. (Invited)

[H] J. Lavrencik, **E. Simpanen**, N. Haghighi, S. Varughese, J. S. Gustavsson, E. Haglund, W. V. Sorin, S. Mathai, M. R. Tan, J. A. Lott, A. Larsson, and S. E. Ralph, "Error-free 850nm to 1060nm VCSEL links: Feasibility of 400Gbps and 800Gbps 8λ-SWDM," *European Conference on Optical Communication (ECOC)*, Dublin, Ireland, September 2019.

[I] A. Larsson, J. S. Gustavsson, E. Haglund, E. P. Haglund, **E. Simpanen**, and T. Lengyel, "VCSEL modulation speed: status and prospects," *Proc. SPIE*, vol. 10938, pp. 36-42, March 2019.

[J] **E. Simpanen**, J. S. Gustavsson, A. Larsson, W. V. Sorin, S. Mathai, M. R. Tan, and S. R. Bickham, "Long-reach 1060 nm SM VCSEL - SMF optical interconnects," *European Conference on Optical Communication (ECOC)*, Rome, Italy, September 2018.

[K] **E. Simpanen**, J. S. Gustavsson, E. Haglund, E. P. Haglund, T. Lengyel, A. Larsson, P. A. Andrekson, W. V. Sorin, S. Mathai, M. R. Tan, and S. Bickham, "1060 nm single and multimode VCSELs for up to 50 Gb/s modulation," *IEEE Photonics Conference (IPC)*, Orlando, FL, USA, pp. 65-66, October 2017.

[L] A. Larsson, J. S. Gustavsson, E. Haglund, E. P. Haglund, T. Lengyel, and **E. Simpanen**, "High-speed VCSELs for OOK and multilevel PAM modulation," *IEEE Photonics Conference (IPC)*, Orlando, FL, USA, pp. 355-356, October 2017.

[M] A. Larsson, J. S. Gustavsson, E. Haglund, E. P. Haglund, T. Lengyel, **E. Simpanen**, and M. Jahed, "VCSEL modulation capacity: Continued improvements or physical limits?," *IEEE Optical Interconnects Conference (OI)*, Santa Fe, NM, USA, pp. 53-54, June 2017.

[N] A. Larsson, J. S. Gustavsson, P. Westbergh, E. Haglund, E. P. Haglund, **E. Simpanen**, T. Lengyel, K. Szczerba, and M. Karlsson, "VCSEL design and integration for high-capacity optical interconnects," *Proc. SPIE*, vol. 10109, pp. 1-6, February 2017. (Invited)

[O] **E. Simpanen**, J. S. Gustavsson, E. Haglund, E. P. Haglund, A. Larsson, W. V. Sorin, S. Mathai, and M. R. Tan, "1060 nm VCSEL for up to 40 Gbit/s data transmission," *International Semiconductor Laser Conference (ISLC)*, Kobe, Japan, September 2016.

[P] A. Larsson, J. S. Gustavsson, P. Westbergh, E. Haglund, E. P. Haglund, and **E. Simpanen**, "High-speed VCSELs for datacom," *European Conference on Optical Communication (ECOC)*, Düsseldorf, Germany, September 2016.

Acknowledgement

A thank you to all of you who have supported me in this work.

I would like to thank my supervisor and examiner Prof. Anders Larsson for his contagious curiosity in photonics, and for always keeping his eye on the future. Thanks to my co-supervisor Johan Gustavsson who shares his knowledge with patience and care. Petter Westbergh taught me how great VCSELs are made and Erik and Emanuel Haglund have always been there for support: in fabrication, characterization and matters big and small - thank you.

I am lucky to have such fantastic colleagues at Photonics and Microwave Electronics Laboratories to discuss, work and laugh with. Special thanks to Lars Lundberg, Mikael Mazur, Sheila Galt and Jörgen Bengtsson for keeping me on track. Thanks to Henric Fjellstedt and Mats Myremark for maintaining and providing me with setup components in the optoelectronics lab, and thanks to the staff of the Nanofabrication Laboratory (NFL) who always keep the machines at best performance and generously share knowledge.

Thanks to our collaborators Mike Tan, Wayne Sorin, and Sagi Mathai at Hewlett Packard Enterprise in Palo Alto, Scott Bickham at Corning Research and Development Corporation in Painted Post, Pierluigi Debernardi at Politecnico di Torino, and Stephen Ralph and Justin Lavrencik at Georgia Institute of Technology in Atlanta, for insightful discussions, contribution to my work, and valued support.

The research on 1060 nm VCSELs was financially supported by the Hewlett Packard Enterprise Innovation Research Program, the Swedish Foundation for Strategic Research (SSF), and the Swedish Research Council (VR). 1060 nm optimized fiber was designed and manufactured by Corning. VCSEL electro-opto-thermal numerical simulations were provided by Pierluigi Debernardi. Georgia Tech contributed with a high-performance test setup with excellent DSP capabilities. VCSEL fabrication was performed at NFL, Chalmers. IQE Europe is acknowledged for supplying the epitaxial VCSEL material.

Ewa Simpanen

Göteborg
March 2020

List of Abbreviations

BCB benzocyclobutene
BER bit error ratio
BW bandwidth
DBR distributed Bragg reflector
DD direct detection
DFB distributed feedback
DMT discrete multitone
DSP digital signal processing
EEL edge-emitting laser
FEC forward error correction
FFE feed-forward equalization
HPC high-performance computing
ICP inductively-coupled plasma
IM intensity modulation
ISI intersymbol interference
LED light-emitting diode
MFD mode field diameter
MM multi-mode
MMF multi-mode fiber
MOCVD metal-organic chemical vapor deposition
MPN mode partition noise
MQW multiple quantum wells
NRZ non-return-to-zero
OI optical interconnect
OOK on-off keying
PAM pulse amplitude modulation
PAM-2 two-level pulse amplitude modulation
PAM-4 four-level pulse amplitude modulation
PECVD plasma-enhanced chemical vapor deposition
POF plastic optical fiber
PRBS pseudorandom binary sequence

PRD partial-response duobinary
QW quantum well
RIE reactive ion etching
RIN relative intensity noise
RTP rapid thermal processor
SM single-mode
SMF single-mode fiber
SNR signal-to-noise ratio
TLM transfer length method (or transmission line model)
UF universal fiber
VCSEL vertical-cavity surface-emitting laser
WDM wavelength-division multiplexing

Table of Contents

Chapter 1

Introduction

Data centers are a base component of Internet infrastructure used for storage, computation and access to data. There is a wide variation in size and complexity of data centers, a simpler one is a small server room and highly advanced is a high-performance computing (HPC) system. These last decades, digital growth has been accommodated by rapid expansion of the number of data centers, many privately owned and maintained. This has led to excessive redundancy in the network, with underutilization of servers and low energy efficiency. With an approximate lifespan of 5 years, many data centers are operating with outdated technology that is in need of update and put high demand on maintenance, thereby causing neglect and costly downtime [1–3]. The massive global traffic consumption and the development of cloud computing now move workload away from small, privately managed, data centers and increase the demand for larger data centers [1, 2, 4–6]. These data centers are often referred to as mega, warehouse, exascale or hyperscale data centers and at the end of 2015 there were 259 located around the world, hosting 21% of all data center servers, 39% of all processing power, 49% of all stored data and 34% of all traffic recorded from all data centers [7].

The number of hyperscale data centers is planned to grow to 485 by 2020 [7], seen in Fig. 1.1. The environmental impact caused by data centers due to energy consumption and emission of green house gases has risen a large public interest in green cooling and power [1–4], and the incentive to optimize utilization and cut energy costs is high for mega data center operators [1, 2, 8]. Many projects are therefore employing new network topologies, virtualization, traffic engineering, power management and renewable energy access as ways to improve energy efficiency and develop into green data centers [1–4, 8]. The

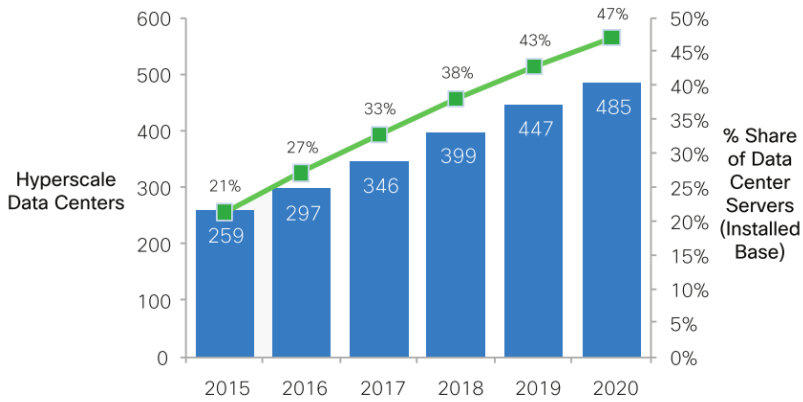

Figure 1.1: Hyperscale data center growth from 2015 to 2020 [7].

aim is to decrease power consumption, increase utilization and control thermal behavior [1] and fiber optics is a key enabler to advance data center technology towards this goal [3].

1.1 Architecture of a Hyperscale Data Center

Hundreds of thousands of servers form the basis of a hyperscale data center. The servers are stacked in racks of about 40 to 80 units, in which they are interconnected via a switch, either Top of Rack or Middle of Rack. Many rack switches are then connected using additional layers of network switches. A hyperscale data center demands careful consideration when building the topology of the switch network. In addition to network throughput, latency, congestion and packet loss [1, 3], the upscaled topology also needs to support a large inter-node communication bandwidth (BW), so that applications can exchange information with remote nodes when needed to then be able to proceed with their local computation. For this purpose, topologies such as the fat-tree was proposed [9], illustrated in Fig. 1.2, and it is designed to spread outgoing traffic from any given instance as evenly as possible among the core switches. The fat-tree topology has been used in large data centers due to its large bisectional BW, economical scalability and backward compatibility [3–5, 8, 9], as well as its fault tolerance and energy efficiency, with low power consumption and heat dissipation compared to a typical, strongly hierarchical design [3]. However, as server performance is improved and the data centers grow larger, the scalability of this topology becomes limited by the

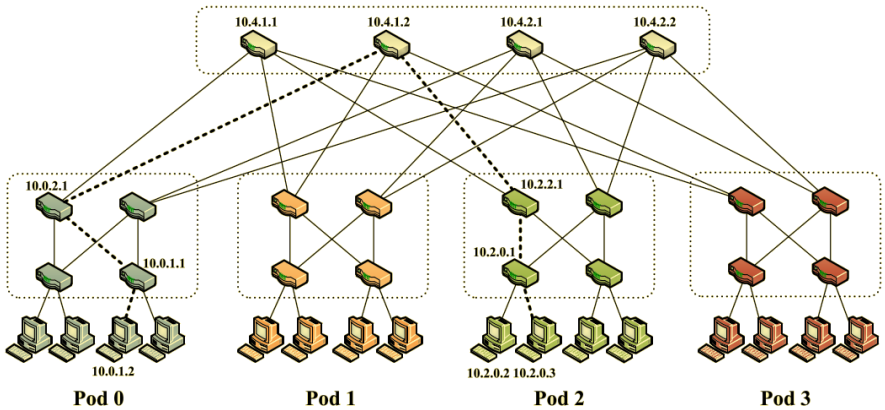

Figure 1.2: Simplified view of a 3-level fat-tree topology. Packets from source 10.0.1.2 to destination 10.2.0.3 take the dashed path [9]. The core layer of switches is on top and it communicates via an aggregation layer of switches to reach any edge switch.

large amount of interconnections, as well as difficulty to minimize total cable length, thereby revealing a need for interconnects operating at higher bit rates and longer reach.

1.2 Data Center Interconnects

Compared to electrical transmission, optical interconnects (OIs) can provide high data rates with large BW, there is little attenuation and since there is no crosstalk or any electromagnetic interference, optical fibers can easily be bundled [10, 11]. OIs are widely employed in HPCs and hyperscale data centers for rack-to-rack and intra-rack communication. The commonly used standard for short reach communication Ethernet, governs local area networks based on electrical and optical links. In 2010, cloud providers adopted Ethernet servers supporting 10 Gb/s lane rates, today hyperscale servers have moved to 25 Gb/s, and they are on their way to move to 50 Gb/s. The advantages of using optical communication puts incentive into developing OIs with shorter reach ($<$5 m) for which electrical standards are typically used [12], and it has enticed research to extend optical operation to connector backplanes and switches. Moving the optical/electrical interface in closer proximity to the electronic chips, or even reducing the number of interfaces, could significantly reduce power consumption as well as communication latency [3, 5], while smaller form factors would help to avoid being limited by frontpanel congestion.

Todays most common OIs use 850 nm vertical-cavity surface-emitting lasers (VCSELs) with multi-mode fiber (MMF) [5]. Commercialized 850 nm OIs can provide 25 Gb/s lane rate up to at least 100 m [12], but if the reach exceeds this limit the OIs suffers greatly from fiber chromatic dispersion and attenuation. Since transmission distance in MMF becomes limited at higher data rates, the OI capacity is further increased by employing parallel lanes to achieve high aggregate link speeds. The Ethernet Roadmap for MMF, in Fig. 1.3, shows that in 2010, 10 Gb/s lanes were integrated to form the 40GBASE-SR4 and 100GBASE-SR10 link standards that reach 150 m, while parallel 25 Gb/s lanes build up to 400 Gb/s aggregate capacity using 16 fiber pairs of 100 m length [13]. The increase in data rate has thereby decreased the link reach length. However, with 100 m link reach, future standards are aiming beyond 400 Gb/s and will be in the Tb/s range, see Fig. 1.4. A possible solution, following up on highly parallel speeds with 100 Gb/s lanes, is 1.6 Tb/s [12, 14, 15]. The high lane rate of 100 Gb/s is realized by using the improved base speed of 50 GBaud, seen at 2018 in Fig. 1.3, together with higher order modulation, in this case four-level pulse amplitude modulation (PAM-4) instead of binary two-level pulse amplitude modulation (PAM-2), which provides double the amount of bits per symbol.

In addition to making use of aggregated multiple parallel lanes and higher order modulation, such as PAM-4, throughput of OIs also benefit from the employment of higher BW fiber such as the move to the fiber standard OM4 (Fig. 1.3), reducing the VCSEL spectral width, adding equalization to the optical transmitter and receiver to compensate the effective BW of the channel, using forward error correction (FEC) to compensate for received errors, other types of digital signal processing (DSP), and/or operating at multiple wavelengths in the same fiber, known as wavelength-division multiplexing (WDM) [16].

With limited reach, 850 nm VCSEL and MMF OIs have been pinpointed a significant bottleneck [6, 17] and hyperscale data centers require a minimum fiber reach of about 500 m [18], and up to 2 km [12]. However, by extending the wavelength of the GaAs-based VCSEL it is possible to drastically reduce the effects of chromatic dispersion and attenuation in the MMF and meet the requirement for longer reach. Further improvements can be made by introducing VCSELs with narrow spectral width to experience less dispersion in MMF or to use in combination with single-mode fiber (SMF). The purpose of this work is to investigate the potential of increasing the operating wavelength of the standard OI, and demonstrate the 1060 nm VCSEL as a light source for high modulation speeds over longer distances. With 1060 nm VCSELs, lane rates of up to 100 Gb/s over fiber up to 2 km are of high interest that could serve to further develop OI standards.

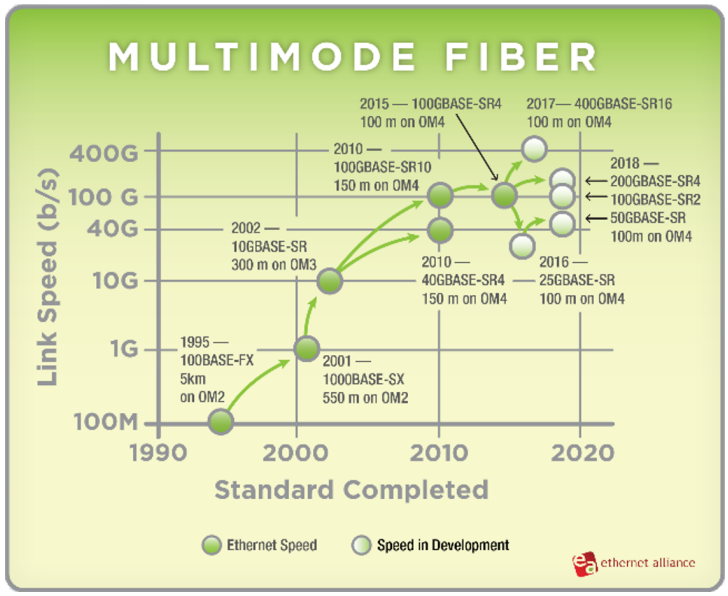

Figure 1.3: MMF Ethernet Roadmap 2016 [13].

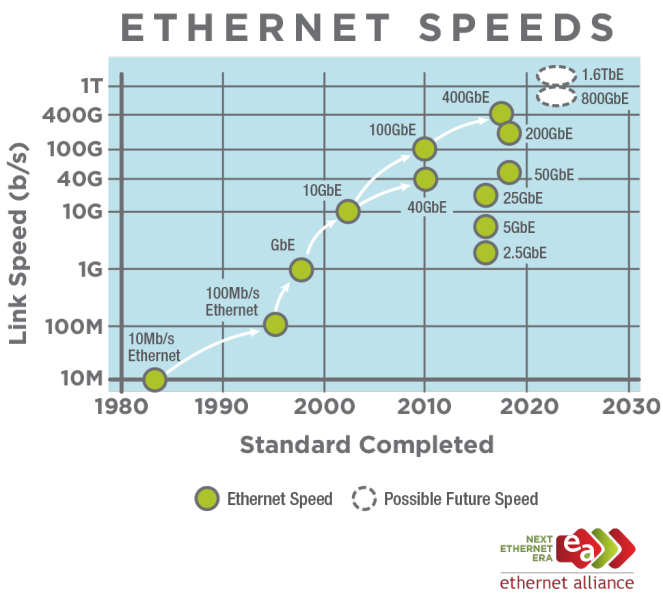

Figure 1.4: Ethernet Roadmap for link speed 2019 [15].

Chapter 2

Optical Interconnect Technologies

The OI transmits and receives data in the optical domain and provides an electrical interface that can connect to electrical equipment such as servers and switches of a data center. The typical VCSEL-based OI transmitter consists of a driver and a VCSEL, as in Fig. 2.1a, and the receiver of a photodetector and an amplifier, in Fig. 2.1b. The driver directly modulates the VCSEL and the output is passed on to an optical fiber, which is then received by the detector and converted back to an electrical signal that is amplified to sufficient levels before entering a demodulator.

Any physical channel has limited BW, adds noise to the signal, and causes other impairments, for instance due to non-linearities of the components. How-

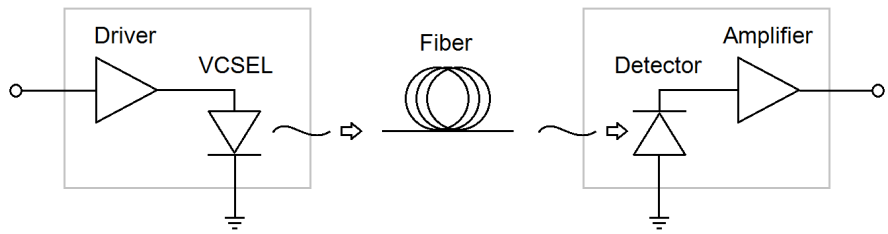

Figure 2.1: The optical channel of a VCSEL-based OI. Input data is applied to the driver that modulates the VCSEL and the resulting optical signal is coupled to the fiber. On the receiver end, a photodetector converts the optical signal back to electrical and the data is then amplified and passed along.

ever, in relative terms, the optical communication channel provides broad BW transmission with low attenuation, while being light weight and having low material cost. In addition, optical fiber is immune to electromagnetic interference, it is electrically insulated, and it provides security of information [19]. OIs enable the high parallelism used in the Ethernet standard. Data centers require bundable cables and transmission with low energy consumption and good thermal properties [1]. As covered in Section 1.1, the interconnects in hyperscale data centers also need to transmit at high bit rates over distances up to 2 km [12], and small size and low cost transceivers are highly desirable.

The alternatives and possible combinations of light source and fiber of an OI is application dependent. Light-emitting diodes (LEDs) can be used in short-range communication systems and have reach over silica fiber in the km range. However, the transmission rate is severely limited and with achievable bit rates in the range of kb/s - Mb/s, they are most often used for local-area-network applications. There is a growing interest in automotive industry to use LEDs together with plastic optical fiber (POF), having benefits of low production and installation cost. High attenuation in POF, makes it most suitable for short distances, in the order of m. For very long distances, sub-Atlantic or inter-city, the light source most often used is the distributed feedback (DFB) laser, operating at wavelengths of 1310 or 1550 nm. For conventional silica fiber, these are the respective wavelengths where the effects of chromatic dispersion and attenuation are very small and together with external modulators and amplifiers, system reach can be up to thousands of km. In hyperscale data center short-reach communication, the need for external modulation and/or amplification is a drawback for many reasons, taking space, drawing power, adding heat, and being costly, to name a few. Even when directly modulating a DFB laser, changing its drive voltage or current to turn it to on and off-states, the energy efficiency is low compared to a VCSEL.

The VCSEL, introduced in Section 2.2, is often considered the ideal light source for OIs, mainly because its design provides a high quality circular beam and possibility for high speed modulation. VCSELs are low-cost devices that can be directly modulated with high power efficiency, and they better allow for fabrication in volume and test-on-wafer. However, it's becoming more and more important to design the VCSEL for high reliability and temperature stability. The VCSEL emission wavelength depends on the semiconductor material system it is based upon. 1310 and 1550 nm VCSELs based on InP compounds suffer from higher current densities for sufficient gain due to high levels of non-radiative recombination in the active region materials [20]. A small refractive index contrast also makes it more difficult to design mirrors with high enough reflectivity at these wavelengths. The 850 nm VCSELs used in short-reach communication standards are GaAs-based. Close to lattice matched $Al_xGa_{1-x}As$ compounds are used in the mirrors and the gain wave-

length can be extended to about 1.1 µm using $In_xGa_{1-x}As$ quantum wells (QWs), without compromising reliability [21].

In most data centers, OM3 and OM4 MMF dominate OIs. However, OM5 is expected to replace OM4 in newly built data centers. These MMF standards differ in effective modal BW, the OM3 has above 2 GHz·km at 850 nm for laser launch, OM4 has a higher requirement of over 4.7 GHz·km at the same wavelength, while OM5 also has the requirement of 4.7 GHz·km at 850 nm, but with the additional requirement of at least 2.47 GHz·km at 953 nm. At the specified wavelengths, the optimized index profile guarantees very low differential mode delay and thereby low intermodal dispersion. This makes OM5 a better option for WDM systems that include longer wavelengths, and it has been shown that the BW of OM5 is sufficient for high-speed transmission (100 Gb/s PAM-4) over 100 m at wavelengths from 850 nm all the way up to 1060 nm (Paper F).

OM3 and OM4 have core diameters of 50 µm, which supports the propagation of multiple transverse modes, as further discussed in Section 2.1. OM5 is available with both 50 and 30 µm diameter cores. The reduced core size still allows for multiple modes, only fewer. The new 30 µm core types of fiber, sometimes referred to as universal fiber (UF), has emerged as an alternative enabling data centers to lay down only one type of fiber, compatible with both multi-mode (MM) and single-mode (SM) transceivers. The UF has a large enough core size to couple all light from a MM transmitter with relaxed enough alignment tolerance, while having a mode field diameter (MFD) of the fundamental mode small enough to match the MFD of a standard SMF [22], which typically has a core diameter of 9 µm.

SMF requires a SM light source but is exempt from mode related impairments such as modal dispersion or mode partition noise (MPN) and can carry transmission over even longer distances. SMF is therefore used to increase data center link reach when necessary. The commonly used MMF is more expensive per unit length than standard SMF but better fiber coupling properties has made them more cost efficient for shorter distances and thus heavily used in data centers [23]. As data centers have grown larger, one needs also to account for the increased number of connectors and links needed with MMF for higher bit rates and extended reach. The most cost-effective solution will depend more on data center architecture and future BW requirements.

2.1 Fiber Propagation

Many of the advantageous properties of OIs are established by the optical fiber. Fibers are often drawn from silica, which is a low cost and light-weight material that has good transmission over a wide range of wavelengths, low losses caused by absorption or scattering, and high resistance to both mechanical and optical

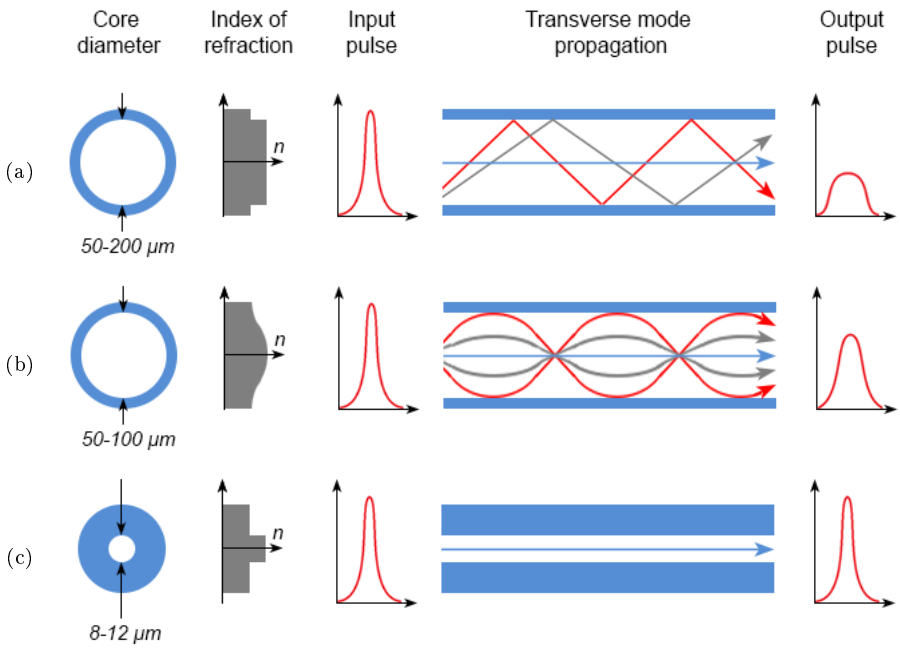

Figure 2.2: Core size, refractive index profile, mode propagation and temporal input/output of a) step-index MMF, b) graded-index MMF, and c) SMF.

damage. The structure of the fiber can be very simple, with a single core having a higher refractive index than its surrounding cladding, relying on total internal reflection to guide light along its length. [24]

With large enough core diameter and refractive index step, the fiber supports several transverse modes, which is illustrated in Fig. 2.2a. A fiber mode is supported if the angle at which light is launched into the fiber satisfies both the condition that it must be small enough for the propagating mode to meet the core-cladding interface at an angle that satisfies the condition for total internal reflection, and so that the distance between reflections inside the fiber allows the field of the propagating wave to repeat itself, and thereby maintain the same transverse distribution and polarization along the length of the fiber. A MMF supports many propagation paths, and lower order modes propagate faster than higher order modes. With longer fiber length the impact of modal dispersion becomes significant and it is important to design the fiber in such a way, that it minimizes the spread in propagation between different modes. By introducing a graded index core, as in Fig. 2.2b, light will instead follow sinusoidal paths down the fiber which helps reduce modal dispersion. It is

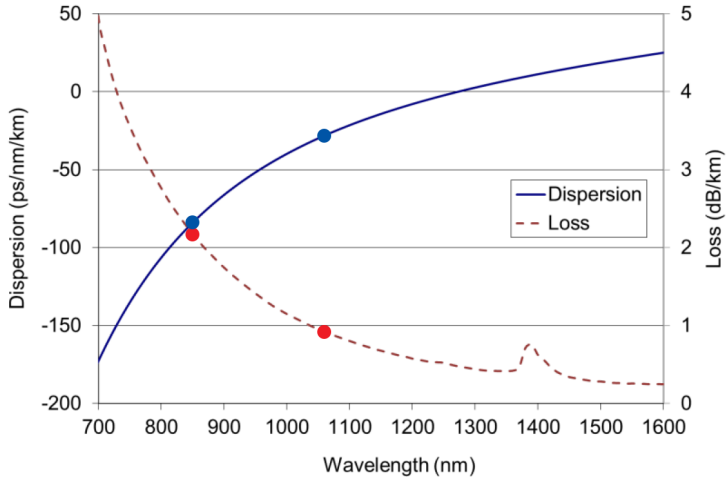

Figure 2.3: MMF chromatic dispersion and attenuation versus wavelength [27].

common for the cores of graded-index fibers to follow a power-law index profile (α profile) and optimize for low differential mode delay with regards to fiber material and propagation wavelength [23]. The index profile can also be designed with an α that varies across the fiber cross-section, and dips and peaks can be used. In Fig. 2.2c, the illustration shows that SMF only supports propagation of the fundamental mode due to its relatively small core size. [24]

Chromatic dispersion and attenuation also limit the reach of fiber transmission and are currently the main constraints of 850 nm OIs [6, 17]. Increasing the operating wavelength reduces these effects. The attenuation in standard silica fiber is 2 dB/km at 850 nm, 1 dB/km at 1060 nm, and 0.2 dB/km at 1550 nm [25]. MMF usually has less than half of the attenuation and only a third of the chromatic dispersion at 1060 nm compared to 850 nm [26], as seen in Fig. 2.3. However, the wavelength is restricted by the light source of the OI, and the GaAs technology limits the VCSEL wavelength to about 1.1 µm [21].

Fiber chromatic dispersion temporally broadens propagating modes due to the wavelength dependency of the refractive index. The extent of pulse broadening depends on the material and the waveguiding, as well as the spectral width and shape of the input pulse. An estimation to determine if a link will be limited by fiber dispersion, D with unit ps/(km·nm), under the assumption of linear broadening and a Gaussian input pulse with narrow spectral width $\Delta\lambda$, is

$$BL|D|\Delta\lambda < 1. \tag{2.1}$$

Thus, for equal launch conditions, with the same initial pulse at the same bit rate, B, the fiber dispersion parameter sets a direct limitation on the allowed transmission distance, L, before bits largely overlap and intersymbol interference (ISI) becomes significant at the receiver end. For SM VCSELs, chromatic dispersion becomes more prominent than for MM VCSELs, for which also modal dispersion and MPN plays part, due to the larger relative broadening.

Noticeable for SM VCSELs under direct modulation are small fluctuations in optical frequency when transitioning between modulation levels, chirp, which adds to the broadening of the pulse. External modulators can produce almost chirp free pulses. One method of reducing the effects of chromatic dispersion in intensity modulation (IM)/direct detection (DD) links, is to use dispersion-shifted fiber, in which the fiber dispersion parameter is designed to minimize effective dispersion for a certain fiber length and wavelength. Optimization of fiber dispersion with regards to VCSEL chirp is further discussed in Section 3.2.

2.2 Oxide-Confined GaAs VCSELs

The VCSEL is a semiconductor laser in which the cavity and the propagation of photons is oriented vertically to the plane of the layers that provide optical gain, as shown in Fig. 2.4a. Due to this geometry, the VCSEL has transverse symmetry and a circularly shaped optical beam. In contrast to an edge-emitting laser (EEL), seen in Fig. 2.4b, the reversed dimensions of the VCSEL, with the short cavity and less restricted lateral size, separates the longitudinal modes and may increase the number of transverse modes. Differently sized VCSELs can be designed with more flexibility and a larger device aperture will result in a more powerful MM VCSEL with a more divergent beam. The vertical geometry also enables on-wafer testing and fabrication of 2D-arrays. [28]

In a VCSEL, the length of material that provides gain inside the cavity is very short. The radiation from stimulated emission is only amplified during a limited part of a cavity round trip. To increase the stimulated emission rate and achieve lasing, multiple quantum wells (MQW) are introduced in the active region. The QWs provide higher gain for equal carrier density compared to bulk material [28]. The mirrors on either side of the active region also need to be highly reflective so that photons will pass several times through the active region before leaving the laser. The semiconductor distributed Bragg reflector (DBR) relies on reflection and transmission of light at interfaces of two different materials having two different refractive indices, a mirror pair. Each layer, being a quarter wavelength thick, reflects light at the interfaces

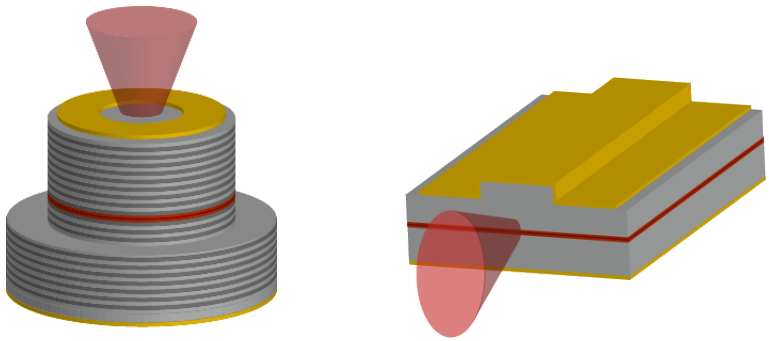

(a) (b)

Figure 2.4: Geometry and optical output direction relative to the orientation of the active region of a) the VCSEL, emitting vertically with a circular beam, and b) the EEL, emitting light along the plane of the layers with an elliptic beam.

that add in phase. These mirror pairs can be stacked and designed to provide power reflectance values close to 100%. About 20 mirror pairs are needed to obtain the required minimum reflectivity of 99.8%. The VCSEL structure is almost in its entirety constituted by the two DBRs. This makes the DBR stack important for the performance of the device. Low strain DBR designs can be realized using $Al_xGa_{1-x}As$ compounds, since the lattice constant of GaAs is very close to that of AlAs. [29]

The many passes of every single photon through the active region of the VCSEL lead to a low threshold current. As for any type of semiconductor laser, the performance of a VCSEL is temperature dependent. The emission wavelength is determined by the cavity resonance wavelength rather than the wavelength of the peak of the gain spectrum, as opposed to a Fabry-Pérot type of EEL. The gain peak is determined by the material composition and layer thicknesses of the QWs in the active region. The performance of the device depends on the spectral alignment (detuning) between gain peak and cavity resonance, which changes with temperature. [28]

The DBRs confine the light in the longitudinal direction of the VCSEL and an oxide-aperture is used for transverse optical and current confinement, which is illustrated in Fig. 2.5. The oxidized layer has a lower refractive index than the non-oxidized layer in the center of the structure. The resulting index-guiding provides transverse optical confinement and determines the number of transverse modes. By reducing the oxide aperture size, the higher order modes can be cut-off and SM behavior can be achieved. The oxide aperture can be formed during fabrication with less complexity than other alternatives for transverse confinement. [28]

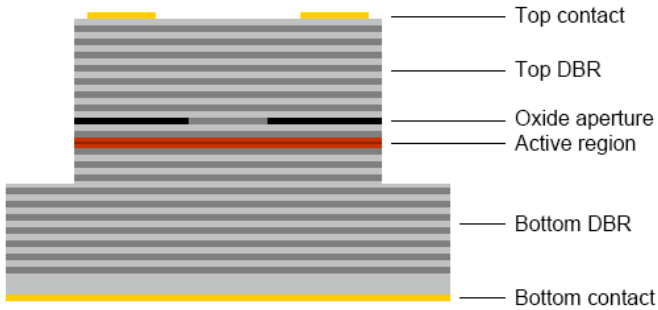

Figure 2.5: Oxide-confined VCSEL.

Further discussion on VCSEL dynamics is presented in the next chapter, Chapter 3, and high-speed VCSEL design is presented in Chaper 4.

Chapter 3

VCSEL Dynamics

VCSELs are key components for OIs in data centers. In the OI, the intensity of the VCSEL is directly modulated by voltage or current which is repeatedly switched between states, representing logical ones and zeros. For high data rates, the VCSEL must be designed to handle very abrupt transitions. The dynamic properties of the VCSEL are governed by the close coupling between carrier and photon densities through stimulated emission. The response to an abrupt change in current is that of a second-order system, with the output power of the VCSEL approaching the new level with a certain rise or fall time while undergoing a damped oscillation, referred to as relaxation oscillation. The rise and fall times and the strength and duration of the oscillation are parameters of great importance for data transfer.

By careful VCSEL design, the OI BW-distance product can be increased. Analysis of the small signal dynamics reveals relations between the modulation response and physical VCSEL design parameters. In extension, the VCSEL large signal dynamics indicate which parameters are limiting transmission performance, in the case that the signal impairments are not dominated by VCSEL or system noise.

3.1 Small Signal Dynamics

The following analysis and related equations are derived from [28].

Insight into the dynamics and speed limitations of VCSELs can be gained by considering the SM rate equations, i.e. assuming a single dominant transverse mode:

$$\frac{dN}{dt} = \frac{\eta_i I}{qV_a} - \left(AN + BN^2 + CN^3\right) - v_g GS, \tag{3.1}$$

$$\frac{dS}{dt} = \Gamma v_g GS - \frac{S}{\tau_p} + \Gamma\beta BN^2, \tag{3.2}$$

where N is the excess carrier density in the active region, η_i the internal quantum efficiency, I the current, q the elementary charge, V_a the active region volume, A the Shockley-Read-Hall recombination coefficient , B the radiative recombination coefficient, C the Auger recombination coefficient, v_g is the group velocity, G the active region gain per unit length, S the photon density in the cavity, Γ the longitudinal confinement factor, τ_p the photon lifetime, and β the fraction of the spontaneous emission that goes into the lasing mode.

The SM rate equations are also applicable to the analysis of the dynamics of index guided MM VCSELs with highly overlapping optical fields and uniform carrier and photon densities. Gain compression is accounted for by writing the optical gain as:

$$G = \frac{G_0}{1 + \epsilon S}, \tag{3.3}$$

where G_0 is the unsaturated gain and ϵ is the gain compression factor.

The following small-signal modulation transfer function can be derived from the SM rate equations by assuming a small modulation current superimposed on a bias current and small changes of the densities from steady state values:

$$H(f) = \text{const} \cdot \frac{f_r^2}{f_r^2 - f^2 + j\frac{f}{2\pi}\gamma}, \tag{3.4}$$

with

$$f_r \approx \frac{1}{2\pi}\sqrt{\frac{v_g g_0 S}{\tau_p\left(1 + \varepsilon S\right)}}, \tag{3.5}$$

where g_0 is the nominal differential gain (dG_0/dN), and:

$$\gamma \approx K f_r^2 + \gamma_0, \qquad \text{with} \qquad K = 4\pi^2\left[\tau_p + \frac{\varepsilon}{v_g g_0}\right], \tag{3.6}$$

where the resonance frequency f_r and the damping factor γ are characteristic parameters of the modulation response. γ_0 is the damping offset and K is referred to as the K-factor. The relaxation frequency that is limiting the modulation BW is close to the resonance frequency. High differential gain,

high photon density and short photon lifetime give a high resonance frequency. A high differential gain is obtained by strained QWs and proper detuning. The photon density and photon lifetime are largely controlled by the reflectivity of the outcoupling DBR. In order to quantify the rate at which the resonance frequency increases with increasing bias current, the D-factor is introduced:

$$f_r = D \cdot \sqrt{I_b - I_{th}}, \quad \text{with} \quad D = \frac{1}{2\pi}\sqrt{\frac{\eta_i \Gamma v_g}{qV_a} \cdot g_0}, \tag{3.7}$$

where I_b is the bias current and I_{th} the threshold current.

The small-signal modulation response can be measured to get an indication of the high-speed performance of the VCSEL. Estimations of the resonance frequency, the damping rate, and the K- and D-factors can then be extracted by a three-parameter fit of the transfer function stated in Eq. 3.4, when multiplied with a transfer function to also account for the effects of parasitics (resistances and capacitances). The modulation BW f_{3dB}, is defined as the frequency where the response in Eq. 3.4 has dropped to half (-3 dB) of its low-frequency value. The modulation BW is limited by either parasitics, thermal effects or damping, or a combination thereof. [30]

Damping flattens the modulation response and increases with photon density, and is also increased by gain compression. Gain compression is caused by gain being reduced at high photon densities because of spectral hole burning and hot carrier effects in the gain region. Spectral hole burning is due to carrier depletion at energy levels involved in the stimulated emission process. Below a few GHz, signal distortion is dominated by spatial hole burning, while non-linear effects of the relaxation oscillation distort the signal at higher frequencies. Maximum distortion occurs at the relaxation oscillation frequency and is strongly related to damping. [31]

Thermal effects limit the BW by reducing differential gain and increasing leakage current from the MQWs at high internal VCSEL temperatures. Self-heating with current in a VCSEL is typically dominated by resistive heating in the DBRs and internal optical loss due to free-carrier absorption. [32] The main parasitic elements of an oxide-confined VCSEL are the resistances in the DBRs and the capacitance associated with charge stored over the oxide layer. An additional capacitance comes from the capacitance under the bond pad, but this can be made much smaller than the oxide capacitance. [33, 34]

SM and MM VCSELs, with emission spectra shown in Fig. 3.1, differ in their dynamic behavior. The SM device has strong non-linear gain suppression, due to higher photon density in the center of the device and strong lateral carrier diffusion, and therefore the modulation relaxation oscillations are more damped. VCSELs can be made SM by reducing the oxide aperture size. Small oxide aperture confines current to a small volume, which lowers the threshold current but causes increased differential resistance, leading to more

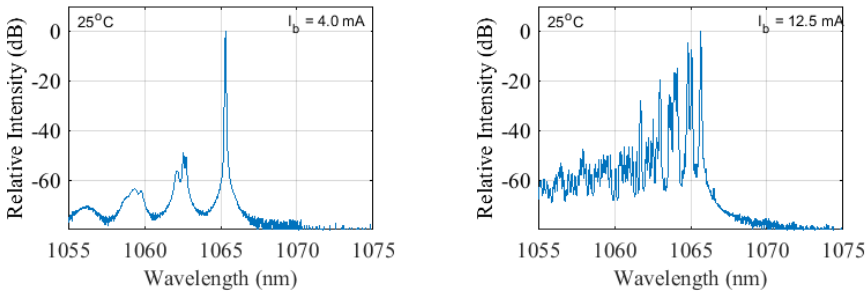

Figure 3.1: Representative spectra for a a) SM VCSEL, and a b) MM VCSEL.

self-heating that results in lower maximum output power. If the tip of the oxide aperture is placed where the optical field is low, the optical confinement is reduced, the mode size increases, and the beam divergence is reduced [35]. The oxide layer can then be made thicker to reduce capacitance. A tapering of the tip can be used for less diffraction loss. The transverse modes of a MM VCSEL are distinguished by their different spatial intensity distributions and resonance wavelengths. A strongly guided cavity increases the number of supported modes and the modes compete for available carriers in the QWs. The individual intensity distributions of the modes make them overlap differently with carrier density in the QWs and give them different modal gain. The modes also experience different loss due to their different extension in the lateral direction. Modes that overlap less with each other have a higher probability to coexist. At higher currents, thermal lensing will squeeze modes together and increase the number of supported modes. Spatial hole burning locally depletes carriers in the QWs, and when carrier drift and diffusion are not enough to replenish the depleted region, other modes may become supported. There are many ways to intentionally change the modal loss or gain and/or use transverse guiding to select lasing modes.

3.2 Large Signal Dynamics

The nonlinear properties of the VCSEL complicate the large signal dynamic response. The optical output depends strongly on the amplitude and frequency of the input signal and resonant and modal distortion can be significant. Numerical simulations derived from the rate equations can be used to model the

highly complex waveforms in order to analyze VCSEL large signal dynamics [36].

Under large signal modulation, such as when a bit sequence is transmitted, the VCSEL operation is switched between states by altering the drive current or voltage. In this work, a set bias current has been chosen as an operating point to which the signal is applied as a voltage swing, of fixed amplitude and frequency, the latter corresponding to the symbol rate. The optical output of the VCSEL is transmitted and then a receiver converts the bits back to electrical voltage levels. The received signal can be captured in time domain and sampled on top of itself to create an illustrative compilation, where the pattern formed represents all possible level transitions, referred to as an eye diagram. Eye diagrams are used to evaluate signal quality and discover system impairments.

3.2.1 Transients

Even with an ideal step input drive signal, the resulting large signal response would experience a certain rise time, overshoot, ringing, and fall time, seen in the illustration of an eye diagram in Fig. 3.2a. The rise and fall times, t_r and t_f respectively, are defined as the time it takes for the signal to increase or decrease between the 10% and 90% signal levels. There is an overshoot on symbol transitions, followed by ringing that eventually settles down, unless the bit rate is fast enough for a consecutive bit symbol to interfere with a new transition, effectively causing ISI. ISI can be observed to close the eyes both vertically and horizontally, thereby respectively acting as a power and a timing penalty. Reduced signal-to-noise ratio (SNR) widens the signal voltage levels, and wider eye crossings are a sign of timing jitter, illustrated in Fig. 3.2b.

The rise and fall times and the strength and duration of the oscillation are parameters of great importance for data transmission, affecting the maximum achievable bit rate. High-speed modulation requires short rise and fall times, e.g. high modulation BW, and a sufficiently damped modulation response for the oscillation to settle before the next bit slot to avoid excessive timing jitter. The presence of a strong resonance peak causes an overshoot on symbol transitions, which can be detrimental especially for multilevel data transmission. It is common to bias and drive the VCSEL so that the off-state current is always above the threshold current, to improve the turn-on behavior and introduce less overshoot and ringing [37]. This also reduces frequency chirp, discussed in the next section, which can be of high importance for SM VCSELs.

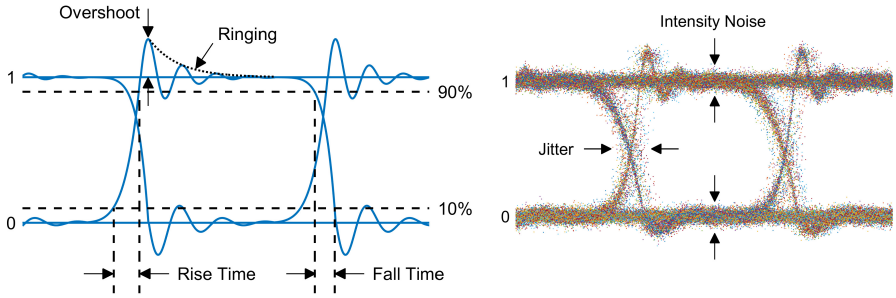

Figure 3.2: Eye diagrams illustrating c) overshoot, ringing, and rise and fall time, and b) timing jitter and amplitude noise, for two-level modulation.

3.2.2 Chirp

As the VCSEL undergoes direct current modulation, the photon density varies, and momentary changes in the carrier population induce fluctuations in the refractive index of the active region. This gives rise to variations in the laser frequency (or wavelength) that broaden the VCSEL spectral width. For SM VCSEL OIs, in which the relative effects of chirp can be significant, this leads to either pulse broadening or compression along a dispersive fiber. The amount of chirp can be quantified by the unitless chirp parameter C that, for a Gaussian pulse, is estimated from the product of the temporal duration (T_0) and the spectral width ($\Delta\omega_0$) at 1/e intensity points, according to

$$T_0 \cdot \Delta\omega_0 = \sqrt{1 + C^2}. \tag{3.8}$$

The chirp parameter can therefore be estimated from measurements of the time-bandwidth product of a short optical pulse from a VCSEL.

When propagating over fiber, the laser chirp and the fiber dispersion will both contribute to additional distortion of the pulse. Under the assumption of Gaussian pulse propagation, and neglecting higher order dispersion, the ratio between the 1/e intensity pulse widths after (T_1) and before (T_0) propagation through a fiber of length L, is given by the broadening factor [38]

$$\frac{T_1}{T_0} = \sqrt{\left(1 + \frac{C\beta_2 L}{T_0^2}\right)^2 + \left(\frac{\beta_2 L}{T_0^2}\right)^2}, \tag{3.9}$$

where β_2 is the group velocity dispersion coefficient, which is related to the fiber dispersion parameter D with unit ps/(nm·km), defined by the inverse group velocity (v_g) variation with wavelength as

$$D = \frac{d}{d\lambda}\left(\frac{1}{v_g}\right) = -\frac{2\pi c}{\lambda^2}\beta_2, \tag{3.10}$$

where c is the speed of light in vacuum and λ is the propagation wavelength.

Opposite signs of the chirp parameter and β_2 in Eq. 3.9, leads to an initial pulse compression followed by pulse broadening. This combination of laser and fiber, therefore result in a minimum pulse width at a certain fiber distance. Dispersion-shifted fiber can be designed to have a specific amount of dispersion at a given operating wavelength. Thus, the effect of chromatic dispersion can be minimized by employing fiber with dispersion that is optimized to the VCSEL chirp for a minimum pulse width occurring at the distance equal to the length of the fiber.

For a non-ideal pulse, undergoing transitions between modulation levels, the momentary chirp induced frequency shifts can vary in magnitude and direction between the beginning and the end of a transition and together with fiber dispersion cause rise and fall times to either increase or decrease [39]. This was observed and analyzed for a 1 km and 2 km SM link in Paper C.

3.3 Noise

The performance of a system is given by receiver sensitivity, which is the amount of optical power needed to operate below a specific bit error ratio (BER). The performance depends on system SNR, which is defined in the electrical domain and is measured as the ratio between average detector photocurrent and the total root mean square noise current. In IM/DD systems, the electrical power is proportional to the square of the optical power and if thermal noise dominates, the BER will improve with increased optical power. However, other sources of noise could be limiting system performance, creating a BER floor. The primary sources of noise in a VCSEL, that limit the bit rate, are spontaneous emission and MPN, quantified as relative intensity noise (RIN) [40]. Intensity noise thereby dominates VCSEL noise limitations imposed on short reach communication systems. VCSEL phase noise becomes of importance in systems that require highly SM sources, such as some sensing applications.

3.3.1 Amplitude Noise

The most fundamental noise sources that contribute to intensity noise in an IM/DD system, and that are independent of fiber, are shot noise, thermal noise and RIN. The shot noise is caused by randomness associated to time intervals between photon absorption and electron-hole generation processes, and thereby adds noise both to the optical signal and to the receiver dark current.

The receiver also adds thermal noise, although the thermal noise level does not increase with signal power such as the shot noise does. RIN originates in the laser. Small amounts of spontaneous emission coupling into lasing modes and randomness associated to carrier generation and recombination processes give rise to RIN. RIN is reduced with current because of the increasing photon density in the active region. It also depends on frequency and at a given bias current it peaks at the VCSEL resonance frequency. Mode competition that gives rise to MPN can increase low frequency RIN of MM VCSELs, since the lasing transverse modes continuously compete for gain in the active region, thereby causing the intensity distribution to randomly fluctuate among the different transverse modes. In transmission, fiber chromatic and modal dispersion, as well as mode selective coupling, enhances the effects of VCSEL MPN and overall RIN [41, 42]. For SM VCSELs, not disturbed by optical feedback, low frequency RIN is low and its peak levels can decrease to reach the shot noise limit as current bias is increased. A more damped VCSEL, also exhibits lower level of RIN (Paper D).

RIN quantifies laser intensity fluctuations as a measure of the optical power variations ($\Delta P(f)$) relative to the average optical power level (P_0). The optical power fluctuations will generate a noise current (ΔI) in the receiver circuit. Hence,

$$RIN(f) = \frac{\langle \Delta P(f)^2 \rangle}{P_0^2} = \frac{\langle \Delta I(f)^2 \rangle}{(\Re \cdot P_0)^2}, \tag{3.11}$$

where $\Re$ is the receiver responsivity. RIN is measured with respect to a finite BW optical system and is given in dB/Hz. The total system noise is recorded as well as the contributions of shot noise and thermal noise of the receiver circuit. The RIN can then be calculated from the measured electrical noise power spectral densities as [43]

$$RIN(f) = \frac{\sigma_{tot}(f) - \sigma_{th}(f)}{(\Re \cdot P_0)^2 \cdot R_L} - \sigma_{shot}, \tag{3.12}$$

where $\sigma_{tot}(f)$, $\sigma_{th}(f)$ are the measured, frequency dependent, total and thermal noise powers, R_L is the receiver load resistance, and σ_{shot} is the shot noise defined as

$$\sigma_{shot} = 2q\Re P_0 \cdot \Delta f, \tag{3.13}$$

where q is the elementary charge and Δf is the receiver BW. An estimation of the thermal noise level, not accounting for frequency dependencies, can also be calculated from

$$\sigma_{th} = \frac{4k_B T}{R_L} \cdot \Delta f, \tag{3.14}$$

where k_B and T are respectively, the Boltzmann constant and the temperature.

3.3.2 Phase Noise

For VCSELs of narrow spectral width, line broadening caused by phase noise can be of relevance. Systems that require spectral purity or coherence are often limited by the phase noise of the source [44]. With the assumption of spontaneous emission into the lasing mode being the source of noise, the linewidth $\Delta\nu$ of the lasing mode can be calculated from the modified Schawlow-Townes formula [45]

$$(\Delta\nu)_{ST} = \frac{R_{sp}}{4\pi N_p}, \tag{3.15}$$

where R_{sp} is the rate of spontaneously emitted photons into the mode and N_p is the photon number in the mode. When also accounting for the amplitude-phase coupling that broadens the linewidth of semiconductor lasers, through the α-parameter (or linewidth enhancement factor) [46], Eq. 3.15 becomes

$$\Delta\nu = \frac{R_{sp}}{4\pi N_p} \cdot \left(1 + \alpha^2\right). \tag{3.16}$$

Expressed in terms of VCSEL parameters, Eq. 3.16 is converted to [28]

$$\Delta\nu = \frac{\left(\Gamma v_g g_{th}\right)^2 \eta_0}{4\pi P_0} n_{sp} \frac{hc}{\lambda} \cdot \left(1 + \alpha^2\right). \tag{3.17}$$

This equation contains the optical confinement factor Γ, the group velocity v_g, the threshold gain g_{th}, the optical outcoupling efficiency η_0, the optical output power P_0, the population inversion factor n_{sp}, and the photon energy hc/λ. The resulting linewidth of a VCSEL depends on intrinsic VCSEL parameters and can be estimated from complex models that include both optical field and gain simulations.

Due to the inverse power dependence of the linewidth in Eq. 3.17, the linewidth-power product $\Delta\nu \cdot P_0$ is often used to characterize VCSEL phase noise, a benefit being that the linewidth-power product is critically dependent on the α-parameter. The α-parameter relates the change in refractive index with carrier density to the change in gain with carrier density as in [46]

$$\alpha = -\frac{4\pi}{\lambda} \frac{\mathrm{d}n/\mathrm{d}N}{\mathrm{d}g/\mathrm{d}N}, \tag{3.18}$$

where λ is the wavelength, n the refractive index, g the gain per unit length, and N the carrier density.

Chapter 4

VCSEL Design and Fabrication

The VCSELs that are presented in this work (Papers A - F) have been designed for 1060 nm to enable high speed and extended reach, as motivated in Chapter 1, by utilizing the improved fiber properties at longer wavelengths, discussed in Section 2.1, while maintaining the benefits of GaAs technology, in Section 2.2.

Design and fabrication of 1060 nm VCSELs is barely established in comparison to 850 nm technology. However, high-speed VCSEL design principles, connecting back to VCSEL dynamics (Chapter 3), are the same at longer wavelengths, which offers flexibility with the possibility of extended use of binary materials since GaAs is non-absorbing at 1060 nm. The design of the active region needs to include strain compensation for the higher In-content, but 1060 nm VCSELs can achieve higher energy efficiency and temperature stability compared to 850 nm devices. The QWs are deeper, which lowers the leakage currents, especially at higher temperatures. The bandgap is reduced, and it is possible to use lower drive voltages. [28, 47]

4.1 1060 nm VCSELs

We have developed two 1060 nm high-speed designs, referred to as D1 and D2, derived from our previous 850 nm designs [48] and [49], respectively. In each design, the epitaxial structure is composed of approximately 400 semiconductor layers with varying thickness, composition and doping. These layers mainly form the active region and the surrounding DBRs, including the oxide layers. The device structure, shown in Fig. 4.1, is a p-side up top-emitting circular double mesa structure encapsulated in benzocyclobutene (BCB). The top mesa defines the size of the oxide apertures and minimizing the diame-

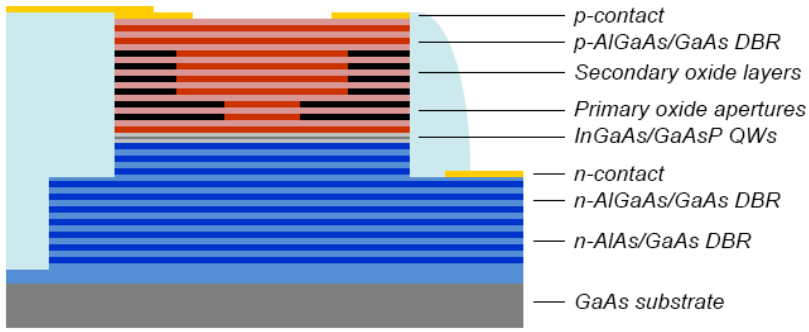

Figure 4.1: Cross sectional view of a 1060 nm oxide-confined GaAs VCSEL structure, showing the top and bottom mesa, active region, oxide apertures, contact placement and BCB planarization.

ter of the top mesa and planarizing the structure with BCB helps to reduce capacitance.

In the active region, the very core of the VCSEL, there are three $In_xGa_{1-x}As$ QWs. The strain in the MQW provides high differential gain, which promotes high speed [47, 50]. There are strain-compensating $GaAs_yP_{1-y}$ barriers between the QWs to reduce the net strain of the active region. Devices containing In in the QWs have also been shown to have good reliability [21]. The designs all use a short half-wavelength cavity to maximize the field intensity over the MQW and promote high speed [50]. This is illustrated in Fig. 4.2a and 4.2b.

The DBRs on either side of the active region consists of low index $Al_xGa_{1-x}As$ and high index GaAs layers. The refractive index difference must be large between the two mirror pair materials to achieve as high reflectivity as possible. To then avoid abrupt potential discontinuities in the DBRs that add resistance to the current injection in the longitudinal direction, the material composition is graded at the interfaces, using continuous grading in the p-DBR and step-grading in the n-DBR. The electrical conductivity is also improved by modulation doping. High doping levels can have a large impact on optical field loss, since photons are absorbed by free-carrier absorption [32]. Modulation doping is used to keep doping levels low in areas where the optical field intensity is high, thereby minimizing internal optical loss, and still be able to have very thin, highly doped regions close to the interfaces, where the intensity of the optical field is low, to gain the benefits of reducing the effective barrier height. AlAs is used as the low index material in the bottom part of the n-DBR to improve thermal impedance. [29]

The emission wavelength of the VCSEL is determined by the cavity res-

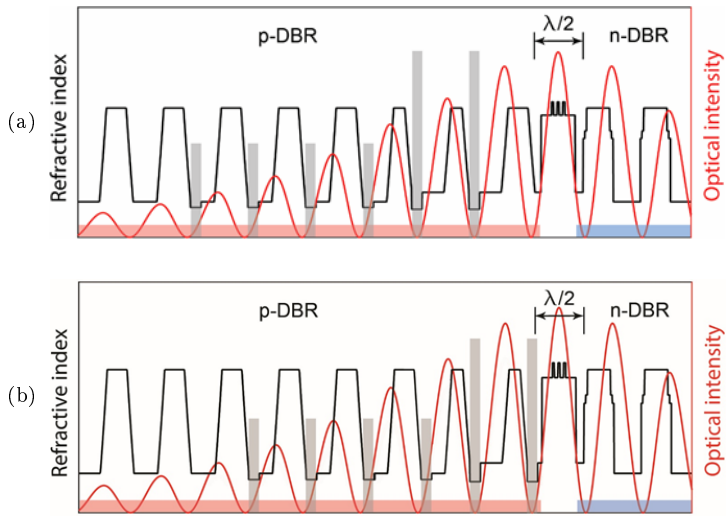

Figure 4.2: Refractive index and optical intensity in the longitudinal direction close to the active region of the VCSEL for Design a) D1, and b) D2. The p- and n-doped DBRs are indicated, as well as the positions of the oxide aperture layers (grey bars).

onance and the wavelength of the gain peak is determined by the material composition and layer thickness of the QWs. The gain peak shifts with temperature a few times faster than the cavity resonance [33, 51]. The increasing misalignment at high current and temperature leads to a saturation of output power. The gain peak is therefore set at a shorter wavelength than the cavity resonance, 1045 nm compared to 1060 nm. The threshold current is highly dependent on the detuning of the cavity resonance and gain peak. The VCSEL design can be optimized for either low threshold current and high power at a specific ambient temperature, or more temperature independent threshold current and output power.

Transverse optical and current confinement is achieved by two primary oxide apertures positioned on the p-side at optical field nodes. Four secondary oxide layers further reduce capacitance over the structure. D1 has oxide layers that are 30 nm thick, while the thinner oxide layers of D2 are 20 nm thick and all placed one mirror pair closer to the active region, see Fig. 4.2. Thin oxides placed at field nodes result in weak optical guiding [52]. D2 therefore has lower beam divergence and reduced spectral width, which is beneficial for long distance transmission [35]. With the primary oxide apertures closer to the active region, transverse carrier confinement improves, which facilitates SM operation.

4.2 Fabrication

The fabrication of the 1060 nm VCSELs was performed in a controlled environment, a cleanroom facility, where contamination from environmental pollutants is limited, interfering UV radiation is filtered out, and the air temperature and humidity are stable. Throughout the fabrication, the samples were also thoroughly cleaned with solvents to reduce the effects of surface contamination.

Only standard processing techniques are required and there is no increase in complexity compared to fabrication of 850 nm VCSELs. The process lithography is relatively insensitive to resolution, requiring µm precision, and was achieved solely by UV photolithography.

The epitaxial growth was done by metal-organic chemical vapor deposition (MOCVD) on an undoped GaAs substrate at IQE Europe. Once the epitaxial material is obtained, it is cleaned and prepared by lithography and an oxide strip (HCl wet etch) for deposition of Ti/Pt/Au p-contact rings and alignment marks using electron beam evaporation, see Fig. 4.3a. A Si_xN_y cap is deposited by sputtering to protect the GaAs surface in the center of the p-contacts, defined by lithography and NF_3 inductively-coupled plasma (ICP) reactive ion etching (RIE), before the top mesa is etched by $SiCl_4$ ICP-RIE, seen in Fig. 4.3b. A second layer of Si_xN_y is deposited, this time by plasma-enhanced chemical vapor deposition (PECVD), and removed from the mesa sidewall by NF_3 ICP-RIE after patterning by lithography. Oxide apertures are then formed by subjecting the sample to wet oxidation at high temperature, as in Fig. 4.3c. Al-rich DBR layers will oxidize at faster rate with increasing Al-content. The oxide aperture sizes are controlled by infrared microscopy and the protective Si_xN_y layers are etched away by NF_3 ICP-RIE.

A fourth lithography step defines the shape of the n-contacts and the surface oxide is again stripped before metal deposition. The electron beam evaporated Ni/Ge/Au n-contacts are annealed in a rapid thermal processor (RTP). The annealing temperature is ramped slowly and is kept below the temperature of the previous wet oxidation. Contact anneal can introduce strain in the VCSEL structure, but it improves the ohmic properties of the contacts. The bottom mesa is formed by lithography and $SiCl_4$ ICP-RIE, see Fig. 4.3d. Transfer length method (or transmission line model) (TLM) test structures on the wafer can now be used to determine the quality of the contact formation.

Si_xN_y is deposited in a thin layer across the surface by PECVD. BCB is then spin-coated onto the sample, exposed, developed and hard cured in an oven. Fig. 4.3e shows the approximate shape of the thick BCB before planarization begins. Multiple lithography steps with various masks are used to first reduce the peak BCB thickness, then open up for the n-contacts and the p-contacts and finally removing the remaining Si_xN_y at the surface. The

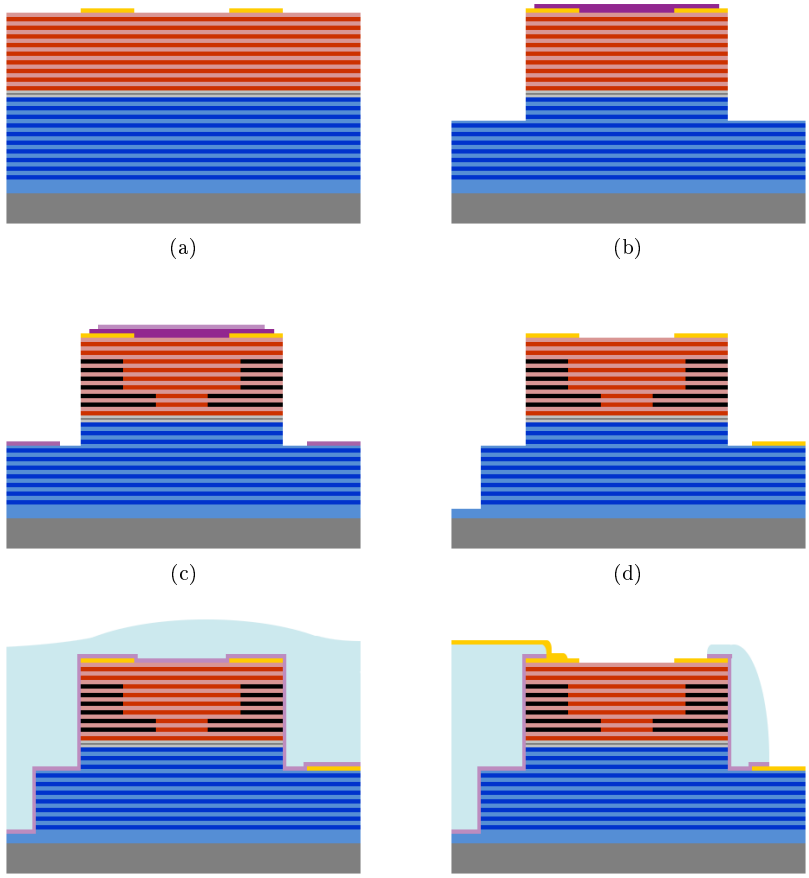

Figure 4.3: The process steps for fabrication of 1060 nm high-speed VCSELs include a) deposition of p-contacts, b) protective Si_xN_y deposition and top mesa etching, c) Si_xN_y masking and oxide aperture formation, d) Si_xN_y removal, deposition of n-contacts and bottom mesa etching, e) Si_xN_y deposition and spin-coating of BCB, and f) BCB planarization, opening of the top mesa surface and contacts, and deposition of contact pads.

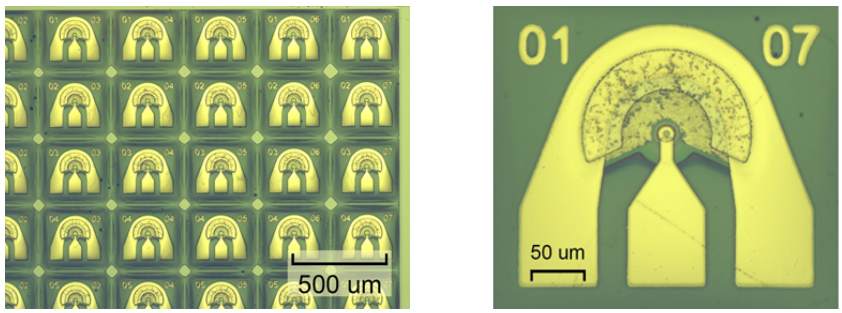

(a) (b)

Figure 4.4: Top view of a) an array of VCSELs, and b) a single fabricated 1060 nm VCSEL.

BCB has an etch rate similar to that of the resist in O_2/CF_4 ICP-RIE. As BCB planarization is complete, Ti/Au contact pads are sputtered on top, see Fig. 4.3f, preceded by lithography and an oxide strip. The final processing fine-tunes the top DBR reflectivity by thinning a GaAs phase tuning layer at the top of the DBR [30] by Ar ion milling.

An array of finished devices is depicted in Fig. 4.4a, and a closer top view of the fabricated VCSEL is seen in Fig. 4.4b. The large contact pads simplify probing with ground-signal-ground probes. The 15 µm diameter top mesa of the VCSEL is indicated by the *p*-contact circle in the center of the image.

Chapter 5

Link Optimization and Throughput Improvement

Increasing the BW-distance product of OIs is a key factor for continued data center growth. Throughput can quickly be scaled by using multiple parallel lanes, higher order modulation, and WDM. Short-reach links can also exploit other forms of modulation or multiplexing, as well as various electrical signal processing strategies to maintain increasing data rates, although available methods are more limited than those used in long-haul systems, due to power, cost and latency constraints in the data centers. Further link improvements can be made by not only choosing the individually best performing OI components, but also optimizing the conditions for their joint operation.

Each component should provide high BW with low loss and low levels of noise, while being highly linear and reliable. Increasing component BWs can yield significant overall link improvement, as in the case of moving from OM2 and OM3 to OM4 and OM5 MMF standards, previously shown in Fig. 1.3 and further discussed in Chapter 2. VCSEL modulation BW dominates link BW and the nonlinear electrical to optical conversion of the VCSEL also presents a significant link impairment. Therefore, the dynamics of the VCSEL, presented in Chapter 3, is of high importance for overall link performance. Because of the bias dependence of the VCSEL's dynamic behavior, the driver is best designed in conjunction with the VCSEL, tuning both the bias point and the voltage swing. At high data rates, the optical power levels need to be optimized for minimizing the nonlinearity. Employing DSP techniques in the transmitter and/or receiver, can help relax BW constraints imposed by the components and maximize the data rate for the available BW.

5.1 VCSEL and Fiber Interaction

The combined VCSEL and fiber performance is of high importance for link optimization. Primarily, the VCSEL wavelength and fiber composition determine the amount of fiber attenuation and chromatic dispersion, which affects the SNR directly and through induced ISI. In MM OIs, modal dispersion arises as relative delays between the fiber modes excited by the VCSEL modes, due to the different optical paths they take in the fiber, as determined by the *alpha*-profile of the MMF. Changes in MMF mode delays can produce advantageous or detrimental effects to the channel BW. The performance of VCSEL-based OIs is also limited by penalties from VCSEL noise that increase with both fiber coupling and transmission. SM VCSEL OIs are exempt from MPN and fiber modal dispersion but are instead more vulnerable to optical feedback, and to the effects of chirp.

5.1.1 Single-Mode and Multimode VCSELs and Fibers

Standard 850 nm MM OIs suffer from numerous penalties. In addition to the limiting fiber chromatic dispersion and attenuation at this wavelength, impairments include RIN (including MPN), selective mode coupling and modal dispersion that all affect the receiver sensitivity. MPN is dependent on optical power and when MPN becomes the dominant noise penalty in a channel, its effect on the SNR degradation cannot be mitigated by simply increasing the transmitted power. For some MM OIs, the MPN penalty is a limiting noise factor for realizing longer reach [53].

The MM VCSELs of MM OIs have the benefit of being more tolerant to optical feedback. Alignment is also much helped by the large fiber core diameter, which has been a cost benefit for MM OIs [23]. MM VCSELs can often be relatively large in size and therefore have a higher power budget that better allows for an increased number of modulation levels. However, a tradeoff with the larger VCSEL size is that it is also often accompanied by increased energy consumption and reduced modulation BW.

Under special coupling conditions the propagation reach in MMF can be dramatically increased [54]. Exciting a limited number of fiber modes reduces the resulting modal dispersion and increases MMF BW. Selective excitation can be realized by launch with an SMF [55]. One can also use VCSELs with fewer transverse modes and thereby excite fewer fiber modes, which has been shown to enable longer transmission distances in MMF, while still retaining the ease of connectorization of MMF [56–58]. The narrower spectral width of a SM VCSEL further improves fiber propagation and enables higher bit rates over longer distances. Compared to MM VCSELs, SM VCSELs do not suffer from mode competition and therefore MPN associated to the VCSEL modes is mitigated. SM lasers are, however, more susceptible to RIN enhancement

due to optical feedback [59] and depending on the launch conditions, higher order fiber modes can still be excited. Proper mode-size conversion when coupling from the VCSEL to the fiber, can make sure SM optical signals are efficiently transmitted along standard graded-index MMF, without any loss of performance compared to using standard SMF [60]. The required MMF tolerances needed to achieve high efficiency SM transmission are no tighter than that for standard SMF coupling and no mode conversion in the MMF occurs [60].

SMF only supports propagation of the fundamental mode and SM OIs are therefore free from all mode induced penalties. Today SMF is used only where longer reach is required and MM OIs have long been considered the most cost effective solution, even though SMF is less expensive per unit length. As the bit rate and transmission distance requirements continue to increase, and form factors become a limiting factor, SM OIs might become the sole solution. Before that happens, few-mode UF might provide flexible OI solutions.

5.1.2 VCSEL-to-Fiber Coupling

High coupling efficiency is important to achieve high SNR. Coupling between the VCSEL and fiber introduces loss but also determines how the VCSEL modes will couple into the modes of the fiber. The number of excited modes and the power distribution between the modes is going to influence the impulse response of the fiber. Optical feedback reflecting back into the VCSEL could also lead to RIN enhancement, especially for SM VCSELs. Transmission reach at a given bit rate can therefore be increased for both SMF and MMF links, by optimization of the launch conditions.

MM OIs have a relatively relaxed alignment requirement between the VCSEL and the large core (50 µm diameter) fiber. Under current modulation, the intensity is distributed unequally between the VCSEL modes and different launch conditions can excite different groups of modes in the fiber, giving rise to unpredictable performance of the MMF. Therefore, it is important to couple as many VCSEL lasing modes as possible into the fiber to avoid signal distortion [61–63]. Reflective feedback can be mitigated by aligning the VCSEL output at an angle to the fiber end. Fig. 5.1a shows the measured coupling efficiency as a function of misalignment between a 1060 nm MM VCSEL and an MMF. The coupling efficiency is above 70% for up to ±10 µm misalignment with respect to the center of the fiber core. Using the same MMF with a SM VCSEL, in Fig. 5.1b, the alignment tolerance is seen to improve.

With MM VCSELs, this overfilled launch is frequently used to excite most of the mode groups in the MMF. Using a short SMF for launch into an MMF will provide a small launching spot that can be radially offset from the MMF core center, giving an enhancement in the fiber BW, even though several modes

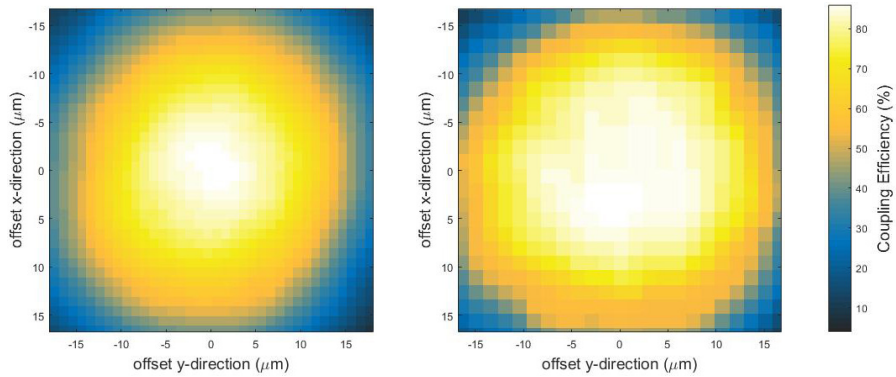

(a) (b)

Figure 5.1: Coupling efficiency versus VCSEL-MMF alignment offset. A short (1 m) OM4 MMF with tilted fiber tip was used to measure the lens coupled power in the fiber from a MM 1060 nm VCSEL with varying offset to the center of the core (position (0,0)). for a) a MM VCSEL, and b) a SM VCSEL.

are excited [55]. This is called offset launch and excites only a subset of all propagating modes of the MMF, which reduces spread in group delays. Higher order mode groups contain more modes than the lower order ones, therefore a majority of the modes can still be excited. Center launch excites very few modes, mainly the the lowest order mode, so that modal dispersion is almost eliminated, assuming that the launch generates a Gaussian near-field injection spot.

SM VCSELs can be used in combination with MMF to further reduce the impact of fiber modal and chromatic dispersion limits the OI BW-distance product. The SM VCSEL has a less divergent output beam which improves coupling efficiency. However, SM VCSELs are more sensitive to optical feedback [61–63]. A larger tilt angle to the MMF can also cause higher order modes to be excited. SM VCSELs can be used to reduce the impact of fiber modal dispersion through selective launch into specific modes groups of the MMF [55, 64]. By proper mode-size conversion, matching the size of the SM VCSEL's Gaussian mode field distribution to that of the lowest-order mode in the MMF, only the fundamental mode will be excited in the fiber, as with the SMF launch.

Coupling from a SM VCSEL to SMF is performed in the same fashion as for the MM OI, tilting the fiber end to reduce optical feedback and optimizing the mode-size conversion. Fig. 5.2a and 5.2b shows transmission eye diagrams

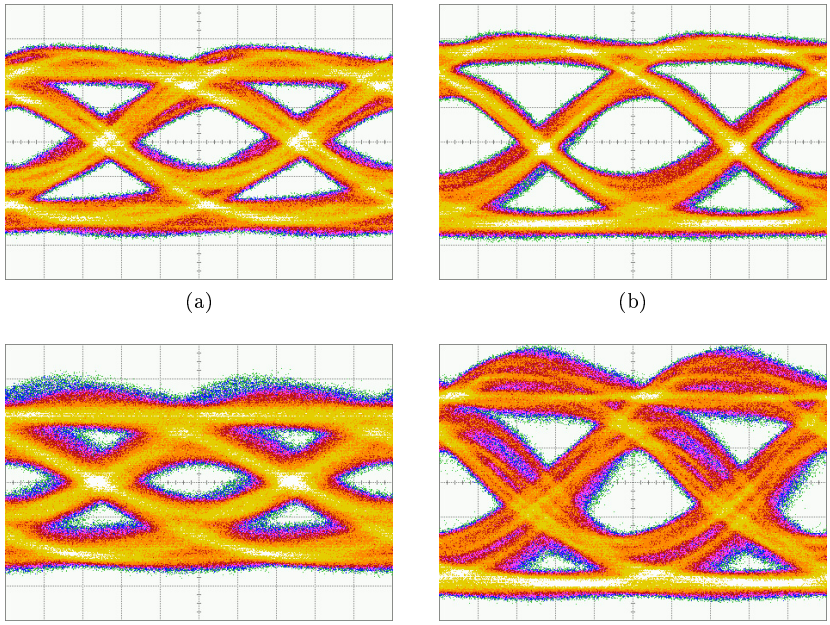

Figure 5.2: Eye diagrams for 40 Gb/s transmission over 100 m MMF with close to matched mode-size conversion for a) a MM VCSEL, and b) a SM VCSEL, and with smaller VCSEL mode field diameter than for the fiber for c) a MM VCSEL, and d) a SM VCSEL.

for close to matched mode-size conversion between the VCSEL and the MMF, and Fig. 5.2c and 5.2d shows the impaired eyes for when the VCSEL spot size near-field, projected on the fiber tip, is smaller than the mode-field diameter of the fiber. However, the smaller core diameter reduces the SM VCSEL-SMF alignment tolerance, as shown in Paper C.

5.2 Modulation

Which modulation format to use is a trade-off between having high spectral efficiency, good sensitivity and low complexity. For an IM/DD system, the available signal space is limited by the fact that only positive values of modulation levels are allowed, due to the nature of the VCSEL requiring positive bias. Data center OIs are also limited in the amount of equalization or FEC that can be used, and therefore most often turn to simple modulation for-

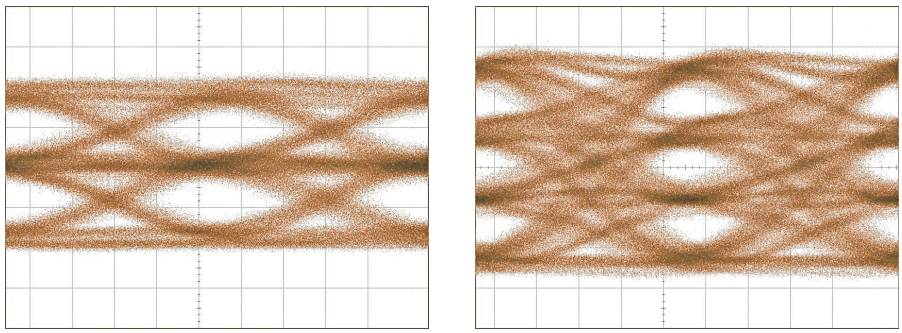

(a) (b)

Figure 5.3: Eye diagrams for a) duobinary, and b) PAM-4 transmission.

mats, designed for high symbol rates. If electronic mitigation techniques for data center OIs were to drastically improve, optimization of more advanced modulation formats for improved sensitivity in IM/DD systems could be considered. Pulse amplitude modulation (PAM) and partial-response duobinary (PRD) are modulation formats of low complexity suitable for high-speed OIs, among which PAM is by far the most popular. 40 Gb/s duobinary and 80 Gb/s PAM-4 eye diagrams are shown in Fig 5.3. Pulse position modulation also has relatively low complexity and is commonly used in wireless infrared communications due to its power efficiency [65], but is associated with a spectral efficiency too low for data center OIs.

During data transmission, the length of the bit sequence can determine the spectral content of the signal. A very long stream of bits will have a higher probability of having several equal symbols in a row, and thus will contain more low frequency components than a shorter bit stream. When characterizing an OI, a pseudorandom binary sequence (PRBS) pattern is often used to emulate the data, and the word length should be representative to the application. A short word length of $2^7 - 1$ is often used with the motivation that data communication links typically use short codes [66]. Increasing the word length can give rise to a significant power penalty for the OI. In Paper B we showed how an increase of the word length to $2^{15} - 1$ introduced a 1 dB penalty to a MM OI, but we saw little deterioration with further increase to $2^{31} - 1$ symbols.

5.2.1 Pulse Amplitude Modulation

PAM is the simplest modulation format applicable for IM/DD systems, such as short-range data center OIs. On-off keying (OOK) is a special case of

PAM, referred to as PAM-2, where the two intensity modulation levels each represent one bit. If the optical modulation amplitude is large enough, higher order modulation formats can be used to increase the transmission bit rates. To improve BW limited VCSEL-based links, various higher order modulation formats have been investigated. An attractive higher order modulation format is PAM-4, with each of the four intensity levels representing two bits, due to low complexity and power consumption. For data centers, the 50 Gb/s lane rate uses PAM-4 since this enables the use of 850 nm MM VCSELs already in production.

As the number of modulation levels increase, as in PAM-4, the spectral efficiency increases. The increased spectral efficiency would primarily enable squeezing more data into the limited electrical BW, without increasing the number of lasers, detectors, and drivers. For a fixed bit rate, the required BW of M-level PAM is reduced by a factor of $log_2(M)$, compared to OOK [67]. With higher order modulation more optical power is required at the receiver in order to achieve the same BER as OOK. Because of the relaxed BW requirements on components, multilevel PAM can be useful in extending the transmission distance, and has been shown to increase the transmission distance in SMF [67].

The possibilities of implementation, advantages and drawbacks of PAM applications in MMF and VCSEL based links were studied in [68–70]. One of the advantages of PAM is the simplicity of implementation. For link testing purposes, PAM-4 can be generated by combining two clock aligned decorrelated binary data streams, where one of the streams must be half of the amplitude of the other. However, reflections in the power combiners in this setup will degrade the generated signal quality, and precise signal phase control and amplitude is also required. A much better way to generate a PAM-4 or possibly PAM-8 signal is to use a dedicated circuit, such as an 8-bit digital to analog converter. Experimental BER measurements with PAM-4 signals can be done in real time using a standard error analyzer designed for OOK. The decision thresholds have to be set between the levels of PAM-4 and the error analyzer has to be programmed with a binary pattern corresponding to transitions of the given PAM decision thresholds. If the measured BER is low, it can be assumed that only symbol errors between neighboring levels occur and the calculation of the resulting BER can be greatly simplified.

The increased number of modulation levels of PAM-4 requires higher SNR to achieve error-free data transmission, which can be derived from observing eye diagrams of higher order modulation PAM signals. An increased number of levels naturally reduces the RIN level that can be tolerated. The presence of a strong VCSEL resonance peak also has a significant effect, as it causes an overshoot on symbol transitions, which can be more detrimental for multilevel data transmission. PAM-4 is therefore often used in combination with

electrical mitigation techniques, presented in the next section.

5.3 Electrical Mitigation Techniques

Power penalties due to ISI caused by the limited BW and nonlinear response of the VCSEL, the fiber modal and chromatic dispersion, and the limited receiver BW, can be detrimental for OIs. Heavy use of equalization, pulse shaping, FEC and/or other forms of DSP, are used to mitigate ISI impairments. This leads to increased complexity, latency, and power consumption. The driver and receiver integrated circuits are the biggest consumers of power in a VCSEL OI. Therefore, extended reach OIs would benefit greatly from improving both VCSEL design (with increased modulation BW, reduced parasitics and improved thermal properties) and fiber performance, to enable system implementations with simple modulation formats and a minimum use of electrical mitigation techniques. Implementation of analog electronic equalization for short-reach data center OIs is a possibility [71, 72], and electronic equalization is also being used in active copper cable to increase the transmission distance and reduce cost [73].

A straightforward way of compensating for the ISI induced power penalty is to add equalization. Feed-forward equalizers (FFE) are commonly used linear equalizers that can be either analog or implemented digitally. FFEs consist of a finite impulse response structure with filter taps that are weighted to compensate for the channel distortion [74, 75]. The tap weights are tuned adaptively to the channel by using a known training signal to match the output to the input signal by a least mean-squares algorithm [76]. The tap spacing either corresponds to the symbol period, or to some fraction of the symbol period and the number of taps of the equalizer is an indication of the cost of implementing the system since it relates to the complexity in analog circuitry required [77, 77]. Equalization can be added at the transmitter and/or receiver, in the form of pre-emphasis or post-compensation, helping to relax BW constraints. A drawback of using equalizers is that they enhance the system noise while correcting channel impairments. Equalizers also add an additional power penalty and there is a trade-off between equalization complexity and power requirements. Hence, it is useful to examine format performance from the perspective of the required bit rate and available channel BW, the figure of merit being the ratio between bit rate and equalized channel BW.

Pulse shaping can help maximize the data rate for the available BW by easing constraints set by BW limitations from components and fiber. However, pulse shaping requires increased processing, especially with advanced multilevel formats and is not often used for data center OIs. Raised-cosine is a common type of pulse shaping that changes how the energy of the signal is distributed to keep it from leaking outside the channel BW. Without the use

of raised-cosine, the modulated signal has a step like waveform in time domain and a *sinc* shape in frequency domain. With raised-cosine pulse shaping applied, the appearance of the waveforms is reversed, the time domain signal is now *sinc*-shaped and the signal's frequency spectrum resembles a step function. The step function frequency response, is a closer match to the overall channel response, which can be viewed as a filter. With a close enough match, little of the signal will be lost during transmission.

FEC can be used to detect and correct a limited number of errors in data that has already been transmitted. This is done by sending redundant error-correcting code along with the data of interest. If the signal is determined to be error-free, the redundant bits are simply removed at the receiver. However, if errors are found in the error-correcting code, corresponding adjustments are made to the received data. A commonly used class of error-correcting code is Reed-Solomon, which is has been used in many communication technologies that have been studied and optimized over many years [78]. Total latency, over-clocking, and implementation penalties need to be considered when choosing an appropriate FEC. FEC used for data center applications can allow for latencies that cannot be accepted for HPCs, where higher speed VCSELs together with equalization under OOK modulation is the more likely solution.

Chapter 6

Long-Reach VCSEL-Based Optical Interconnects

The need for extended reach OIs has led to developments that build upon the standard 850 nm VCSEL-MMF technology. Short-reach OIs most commonly employ MM VCSELs and high modal BW OM4 MMF due to its cost and power efficiency [79]. With simple binary modulation and no use of DSP to increase capacity, these links have a reach limited to about 100 m at 25-28 Gb/s [16, 80]. Reach is limited by fiber chromatic dispersion and attenuation at high bit rates. At 850 nm, fiber chromatic dispersion is as high as -85 ps/(nm·km), and fiber attenuation exceeds 2 dB/km [25].

If the optical modulation amplitude is large enough, higher order modulation formats can be used to increase the transmission bit rates. With PAM-4, 50-56 Gb/s can be achieved over 100 m OM4 MMF [16, 80]. PAM-4 and other advanced modulation formats can be used together with pre-emphasis, equalization, and FEC. Heavy use of FEC and other forms of DSP is used to mitigate impairments caused by the limited BW and non-linear response of the VCSEL, the fiber modal and chromatic dispersion, and the limited receiver BW. This leads to increased complexity, latency, and power consumption. In addition to improved VCSEL design (with increased modulation BW, reduced parasitics and improved thermal properties), extending reach would benefit from improved fiber performance to enable system implementations with simple modulation formats and a minimum of DSP.

The VCSEL-MMF link reach can be improved by using MMF exhibiting modal-chromatic dispersion compensation properties or SM VCSELs with a narrow spectral width [81]. SMF with SM VCSEL is an option for very long reach but the transceiver cost is higher due to tight alignment tolerances [23]. The fiber performance in terms of chromatic dispersion and attenuation im-

proves at longer wavelengths [25]. The ideal wavelength is 1310 nm where chromatic dispersion is near zero and attenuation of MMF is only about 0.4 dB/km. However, the GaAs-based VCSEL technology, which is superior to the InP-based in terms of speed, efficiency, manufacturability, and cost-efficiency, can only be extended to about 1100 nm using conventional compound semiconductors without compromising reliability [82]. This has created an interest in GaAs-based VCSELs at wavelengths just below 1100 nm where the fiber chromatic dispersion is -30 ps/(nm·km) and attenuation is below 1 dB/km [25]. These are large improvements with respect to 850 nm. This justifies the development of GaAs-based 1060 nm SM and MM VCSELs for OIs employing SMF or MMF. When MMF is used, the refractive index profile of the fiber must be optimized to minimize the differential mode delay for high modal BW at the operating wavelength.

6.1 850 nm Links

A summary of previously published work on VCSEL-based OIs for extended reach is presented in Paper B, starting with 850 nm VCSEL-MMF links. At 850 nm, 56 Gb/s PAM-4 was enabled over 200 m with modal-chromatic dispersion compensated OM4 fiber using equalization and FEC [83]. SM VCSELs with narrow spectral width have achieved 25 Gb/s OOK over 1300 m OM4 fiber without equalization or FEC [64], 54 Gb/s OOK over 2200 m OM4 fiber with equalization and FEC [84], 49 Gb/s transmission over 2200 m OM4 fiber using discrete multitone (DMT) modulation and FEC [85], and 135 Gb/s DMT over 550 m OM4 fiber with equalization and FEC [86]. More limited reach extension at high data rates has been demonstrated with MM VCSELs by improving VCSEL parameters such as modulation BW, rise and fall times, and intensity noise, and using techniques such as equalization and FEC, and advanced modulation formats. This includes 60 Gb/s OOK over 107 m OM3 fiber using equalization (no FEC) [87], 64 Gb/s PAM-4 over 2000 m OM4 fiber using equalization and FEC [88], and 100 (70) Gb/s duobinary PAM-4 over 300 (500) m OM4 fiber with equalization and FEC [89]. In addition, shortwave wavelength division multiplexing with 4 channels (SWDM4) has demonstrated 212 Gb/s (4 x 53 Gb/s PAM-4) and 400 Gb/s (4 x 100 Gb/s PAM-4) over 300 and 105 m of wideband MMF, respectively, both using equalization and FEC [90, 91], and 176 Gb/s (4 x 44 Gb/s OOK) over 100 m OM4 fiber using equalization but no FEC [82]. Using OM5, 100 Gb/s PAM-4 over 400 m with FEC has been demonstrated [92].

6.2 Long Wavelength Links

For the purpose of extending the wavelength without compromising reliability [21], GaAs-based VCSELs up to 1100 nm have been developed. Extending the wavelength towards the upper limit of the GaAs-based material system, where optical fiber properties are much improved with respect to 850 nm, could bring the same advantages in terms of cost and power efficiency to long-reach OIs as the GaAs-based VCSEL technology has done to standard short-reach OIs.

The first reports on near 1100 nm VCSELs came from NEC. Using strained InGaAs/GaAs QWs with doped barriers for high differential gain and reduced gain compression, and implantation to reduce capacitance, oxide-confined MM VCSELs at 1090 nm with a modulation BW of 20 GHz and transmission capacity of 25 Gb/s OOK were demonstrated in 2006 [93]. With strained InGaAs/GaAsP QWs, the high temperature performance was improved and 25 Gb/s OOK data transmission at 100^{o}C was demonstrated [21]. The oxide aperture was also replaced by a buried-tunnel junction, which allows for current injection through an intra-cavity n-GaAs layer for low resistance [94]. With a BW of 24 GHz, this VCSEL enabled data transmission at 40 Gb/s OOK [95].

Work on 1060 nm VCSELs has been conducted at UC Santa Barbara. Using strained InGaAs/GaAs QWs with doped barriers and multiple oxide apertures for low capacitance, bottom-emitting VCSELs with a BW of 18 GHz and operation at 25 Gb/s OOK [96] were demonstrated. The data rate was extended to 30 Gb/s using pre-emphasis and FEC [97]. However, most of the work on 1060 nm VCSELs has been conducted by Furukawa [98]. Using double intra-cavity contacts and a dielectric top DBR, low-resistance high-efficiency oxide-confined VCSELs with a modulation BW of 20 GHz were demonstrated. This enabled transmission at 25 and 28 Gb/s OOK over 1000 and 500 m of 1060 nm optimized MMF, respectively [26, 99, 100]. With VCSELs from Furukawa, Georgia Tech demonstrated 50 Gb/s PAM-4 transmission over 310 m of wideband MMF using pre-emphasis and FEC [101]. Finally, Hewlett Packard Enterprise have demonstrated 990-1065 nm oxide-confined, bottom emitting, and lens-integrated VCSELs with strain-compensated InGaAs/GaAsP QWs and transmission at 25 Gb/s OOK over 75 m of OM3 fiber [102]. They also recently demonstrated 25 Gb/s OOK and 50 Gb/s PAM-4 transmission over 2000 m of standard SMF using a SM version of the 1065 nm VCSEL and FEC [103].

At the somewhat shorter wavelength of 980 nm, where the improvements of fiber chromatic dispersion and attenuation are not as large, very small aperture oxide-confined VCSELs with a modulation BW exceeding 30 GHz were demonstrated recently [104]. With a larger aperture size, data transmission at 50 Gb/s up to 75^{o}C was achieved [105].

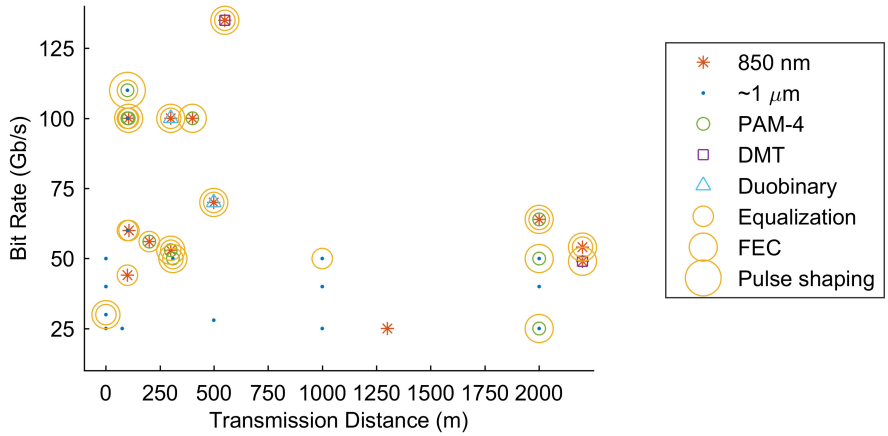

Figure 6.1: OI development towards higher bit rates and extended reach.

Long wavelength InP-based single-mode VCSELs for longer reach single-mode fiber interconnects have reached data rates of 40 Gb/s at 1525 nm [106] and 30 Gb/s at 1270 nm [107] under OOK modulation without equalization. With transmitter and receiver equalization, 56 Gb/s transmission at 1530 nm was recently demonstrated [108].

6.2.1 Contribution to State-of-the-Art

In Papers A to C, we present the design and performance of our 1060 nm oxide-confined VCSELs with strain-compensated InGaAs/GaAsP QWs, using PAM-2 and no DSP. At the time of publication, Paper A reported record modulation speed SM VCSELs at 50 Gb/s, measured at room temperature, and 40 Gb/s at 85^{o}C. With increased maturity, GaAs VCSELs of extended wavelength have potential to achieve even higher intrinsic speeds. In comparison, our much developed 850 nm VCSEL design has pushed the modulation BW to 30 GHz [109] and enabled data transmission at 57 Gbit/s under OOK modulation without equalization [110].

In Paper B, preliminary data transmission experiments show 25 Gb/s over 1 km 1060 nm optimized MMF using a SM VCSEL, but further improvements can be expected by optimizing launch conditions. The narrow spectral width of the SM VCSEL reduces the effects of chromatic dispersion, and in Paper C, we reported a SM OI of error-free 40 Gb/s performance over 1 and 2 km (80 Gb/s·km) of SMF with a cutoff wavelength shorter than that of the standard SMF, without equalization, FEC, or other forms of DSP. The significance of

these results is highlighted in Fig. 6.1, where they are put into context with results from both 850 nm and extended wavelength development for longer reach, and the simplicity of these 1060 nm links stands out. In Paper C, the VCSEL technology employs weak transverse confinement of the optical fields and strong transverse confinement of the current to promote SM operation. The effects this has on VCSEL noise performance is investigated in Paper D.

Transmitter pre-emphasis applied to the SM OI presented in Paper C, increased the error-free PAM-2 bit rate to 50 Gb/s over 1 km in Paper E. The results suggest that the GaAs-based VCSEL technology could potentially bring the same advantages in terms of cost and power efficiency to long-reach SM OIs as it has done to short-reach MM OIs at 850 nm.

In line with MM OI standards, Paper F demonstrates PAM-4 transmission over 100 m OM5, error-free at 100 Gb/s using only transmitter equalization, and up to 110 Gb/s with transmitter equalization and pulse shaping. This shows the feasibility of WDM links utilizing the spectral range from 850 nm all the way up to 1060 nm.

6.3 Future Outlook

The goal of improving the BW-distance product of OIs, must be done with solutions of low cost and low energy consumption and small transceiver footprint. Researchers are also investigating the possibilities of co-packaged highly integrated transceivers, mounted close to heat generating electrical circuits in servers and switches. Performance and reliability at high temperatures are then of utmost importance. Every bit of improvement to the VCSEL performance in terms of BW and noise is also of significant value to overall OI performance.

Optical fibers are being developed with wide BW for longer wavelengths, although they are not yet targeting use at wavelengths above 1 um. The benefits of GaAs VCSELs at these longer wavelengths and of the aggregated capacity of WDM links, might serve as motivation to introduce fiber standards for extended wavelengths. The introduction of a standardized UF would also increase flexibility of data center OI networks.

SM VCSEL designs that still allow for relatively large mode volumes could allow for long-distance transmission without being limited by the power budget. A large size and low resistance VCSEL with high suppression of higher order modes can be obtained by mode filtering [111], and to some extent by epi-design. A low resistance high-power SM VCSEL has potential to perform well in PAM-4 transmission over both MMF and SMF, and transmitter pre-emphasis or equalization could be used to further increase capacity.

Chapter 7

Summary of Papers

Paper A

"1060 nm single-mode vertical-cavity surface-emitting laser operating at 50 Gbit/s data rate," *Electronics Letters*, vol. 53, no. 13, pp. 869-871, June 2017.

In this paper we demonstrated a 1060 nm VCSEL capable of 50 Gb/s transmission, and 40 Gb/s at high temperature, under direct current modulation using the PAM-2 (non-return-to-zero (NRZ)-OOK) modulation format. These first results showed record speed for near 1.1 µm GaAs VCSELs and the VCSEL energy dissipation was as low as 100 fJ/b at high bit rates.

My contribution: I fabricated the VCSELs. The new designs required initial effort to validate the epitaxial growth and adapt the fabrication process. I performed material tests, determined oxidation rates, etch rates, made simulations, designed new photolithography masks and adjusted all process steps. I performed all measurements, analyzed the results and wrote the paper.

Paper B

"1060 nm VCSELs for long-reach optical interconnects," *Optical Fiber Technol.*, vol. 44, pp. 36-42, August 2018. (Invited)

In this invited paper, we present the results from an experimental study of 1060 nm SM and MM VCSELs fabricated from two different epitaxial designs. Both designs use oxide apertures for transverse current and optical confinement, but differ primarily in terms of the positioning of the oxide apertures with respect to the active (gain) region and therefore in terms of current spreading under the apertures. The SM VCSEL is used to transmit data at 25 Gb/s PAM-2 over 1 km 1060 nm optimized MMF without equalization or FEC. This paper also includes an extensive summary of previous development and state-of-the-art regarding extended-reach OIs and near 1.1 µm VCSELs.

My contribution: I fabricated the VCSELs, performed all measurements and processed the data. Thanks to my hard work in the measurement lab we managed to obtain error-free transmission over 1 km at 25 Gb/s. This required investigations to determine the optimum modulation conditions for different VCSEL designs and compare their performance. I also designed plots and figures and co-authored the paper.

Paper C

"1060 nm single-mode VCSEL and single-mode fiber links for long-reach optical interconnects," *IEEE J. Lightwave Technol.*, vol. 37, no. 13, pp. 2963-2969, July 2019.

In this paper, we demonstrate error-free 40 Gb/s PAM-2 transmission over 2 km prototype 1060 nm SMF using a 1060 nm SM VCSEL. The VCSEL intensity noise and frequency chirp are investigated due to their limiting effect on reach. It is also shown that the negative chromatic fiber dispersion at 1060 nm leads to chirp-induced pulse compression over the first about 1.5 km, which helps to extend reach.

My contribution: I fabricated the VCSELs, performed all static and dynamic characterization including large-signal experiments with the SMF, processed all data, analyzed and discussed the results and wrote the paper. The work on RIN and especially VCSEL frequency chirp required extensive efforts in order to obtain the measured results, such as building several new setups including a piezo-controlled stage for fiber alignment.

Paper D

"Noise properties of single-mode VCSELs: Dependence on current confinement and optical loss," submitted to *IEEE J. Quantum Electron.*, January 2020. (Manuscript)

In this paper we present the results from an experimental study of the intensity and phase noise of SM VCSELs. The RIN and the linewidth are measured for VCSELs that differ in terms of transverse current confinement and optical loss. It is shown that the optical resonator loss has a significant effect on both intensity and phase noise while noise is not affected by transverse current spreading. The data analysis is supported by optical gain and resonator calculations to predict the linewidth and estimate the linewidth enhancement factor.

My contribution: I fabricated the VCSELs, performed all measurements, processed the data, and wrote the paper. In a project I proposed, initial tests were performed by an exchange student under my supervision. The study included close collaboration with Politecnico di Torino.

Paper E

"Pre-emphasis enabled 50 Gbit/s transmission over 1000 m SMF using a 1060 nm single-mode VCSEL," *Electronics Letters*, vol. 54, no. 20, pp. 1186-1187, October 2018.

In this paper, we demonstrate an increase of the capacity of the 1060 nm SM VCSEL and SMF link to 50 Gb/s over 1 km using two-tap feed-forward equalization (FFE). This is achieved without FEC or any other form of DSP.

My contribution: I fabricated the VCSELs, performed the static and small-signal characterization, advised on and helped build the transmission experiment setup, performed device and fiber selection, optimized VCSEL drive conditions, contributed to the analysis and in writing the paper.

Paper F

"Error-free 100Gbps PAM-4 transmission over 100m OM5 MMF using 1060nm VCSELs," *Optical Fiber Communications Conference and Exhibition (OFC)*, San Diego, CA, USA, paper M1F.3, March 2019.

In this paper, we demonstrate error-free PAM-2 transmission up to 60 Gb/s and error-free PAM-4 transmission up to 110 Gb/s over 100 m wideband MMF using a 1060 nm MM VCSEL and transmitter equalization and pulse shaping. The results show that the GaAs-based VCSEL technology can be used for wavelength multiplexed OIs with wavelengths from 850 to 1060 nm to enable cost and energy efficient Tb/s interconnect capacity.

My contribution: I fabricated the VCSELs, performed initial static and dynamic characterization of the devices, defined tests to perform, and participated in the transmission experiments at Georgia Tech. Together we used my expertise on the VCSEL behavior and Lavrencik's knowledge and experience with link optimization. I also contributed in writing the paper.

References

[1] X. Jin, F. Zhang, A. V. Vasilakos, and Z. Liu, "Green data centers: A survey, perspectives, and future directions," *CoRR*, no. 1608.00687, Aug 2016.

[2] S. Mittal, "Power management techniques for data centers: A survey," *CoRR*, no. 1404.6681, April 2014.

[3] K. Bilal, S. U. R. Malik, O. Khalid, A. Hameed, E. Alvarez, V. Wijaysekara, R. Irfan, S. Shrestha, D. Dwivedy, M. Ali, U. S. Khan, A. Abbas, N. Jalil, and S. U. Khan, "A taxonomy and survey on green data center networks," *Future Generation Computer Systems*, vol. 36, pp. 189–208, July 2014.

[4] L. A. Barroso, J. Clidaras, and U. Hölzle, "The datacenter as a computer: An introduction to the design of warehouse-scale machines," *Synthesis Lectures on Computer Architecture*, vol. 8, no. 3, pp. 1–154, 2013.

[5] C. Kachris, K. Kanonakis, and I. Tomkos, "Optical interconnection networks in data centers: Recent trends and future challenges," *IEEE Comm. Magazine*, vol. 51, no. 9, pp. 39–45, September 2013.

[6] C. Kachris and I. Tomkos, "A survey on optical interconnects for data centers," *IEEE Comm. Surveys Tutorials*, vol. 14, no. 4, pp. 1021–1036, April 2012.

[7] Cisco, "Cisco Global Cloud Index: Forecast and methodology, 2014-2019," Tech. Rep., 2016.

[8] L. Wang, F. Zhang, J. A. Aroca, A. V. Vasilakos, K. Zheng, C. Hou, D. Li, and Z. Liu, "GreenDCN: A general framework for achieving energy efficiency in data center networks," *IEEE J. on Sel. Areas in Communications*, vol. 32, no. 1, pp. 4–15, January 2014.

[9] M. Al-Fares, A. Loukissas, and A. Vahdat, "A scalable, commodity data center network architecture," *Proc. ACM SIGCOMM*, vol. 38, no. 4, pp. 63–74, October 2008.

[10] G. Liu, J. Gao, H. Cheng, H. C. Wu, E. Lau, L. Yuan, and C. Krause, "Thunderbolt interconnect; Comparing optical and copper approaches," *IEEE International Symposium on Electromagnetic Compatibility Signal/Power Integrity (EMCSI)*, pp. 305–309, August 2017.

[11] H. Cheng, J. Gao, H. C. Wu, G. Liu, E. Lau, L. Yuan, and C. Krause, "Optics vs. copper; From the perspective of Thunderbolt 3 interconnect technology," *China Semiconductor Technology International Conference (CSTIC)*, March 2016.

[12] Y. Sun, "Recent advances for high speed short reach optical interconnects for datacom links," *IEEE CPMT Symposium Japan (ICSJ)*, pp. 63–65, November 2017.

[13] E. Alliance, "The 2016 Ethernet roadmap," http://ethernetalliance.org/roadmap, accessed 2018-02-19, 2016.

[14] C. Cole, "Beyond 100G client optics," *IEEE Comm. Magazine*, vol. 50, no. 2, pp. 58–66, February 2012.

[15] E. Alliance, "The 2019 Ethernet roadmap," https://ethernetalliance.org/technology/2019-roadmap/, accessed 2020-01-24, 2019.

[16] J. A. Tatum, D. Gazula, L. A. Graham, J. K. Guenter, R. H. Johnson, J. King, C. Kocot, G. D. Landry, I. Lyubomirsky, A. N. MacInnes, E. M. Shaw, K. Balemarthy, R. Shubochkin, D. Vaidya, M. Yan, and F. Tang, "VCSEL-based interconnects for current and future data centers," *IEEE J. of Lightwave Techn.*, vol. 33, no. 4, pp. 727–732, February 2015.

[17] C. F. Lam, H. Liu, B. Koley, X. Zhao, V. Kamalov, and V. Gill, "Fiber optic communication technologies: What's needed for datacenter network operations," *IEEE Comm. Magazine*, vol. 48, no. 7, pp. 32–39, July 2010.

[18] A. Ghiasi, "Large data centers interconnect bottlenecks," *Optics Express*, vol. 23, no. 3, pp. 2085–2090, February 2015.

[19] G. Ezeh, "Efficiency of optical fiber communication for dissemination of information within the power system network," *IOSR J. of Computer Engineering*, vol. 12, pp. 68–75, January 2013.

[20] S. J. Sweeney, A. F. Phillips, A. R. Adams, E. P. O'Reilly, and P. J. A. Thijs, "The effect of temperature dependent processes on the performance of 1.5-µm compressively strained InGaAs(P) MQW semiconductor diode lasers," *IEEE Photonics Techn. Letters*, vol. 10, no. 8, pp. 1076–1078, August 1998.

[21] H. Hatakeyama, T. Anan, T. Akagawa, K. Fukatsu, N. Suzuki, K. Tokutome, and M. Tsuji, "Highly reliable high-speed 1.1-µm-range VCSELs with InGaAs/GaAsP-MQWs," *IEEE J. of Quantum Electronics*, vol. 46, no. 6, pp. 890–897, June 2010.

[22] X.Chen, J. E. Hurley, J. S. Stone, A. R. Zakharian, D. Coleman, and M.-J. Li, "Design of universal fiber with demonstration of full system reaches over 100G SR4, 40G SWDM, and 100G CWDM4 transceivers," *Optics Express*, vol. 24, no. 16, pp. 18 492–18 500, August 2016.

[23] R. E. Freund, C. A. Bunge, N. N. Ledentsov, D. Molin, and C. Caspar, "High-speed transmission in multimode fibers," *IEEE J. of Lightwave Techn.*, vol. 28, no. 4, pp. 569–586, February 2010.

[24] S. Gupta, *Textbook on optical fiber communication and its applications*. New Delhi, India: Prentice-Hall of India Pvt. Limited, 2004.

[25] M.-J. Li, "Novel optical fibers for data center applications," *Proc. SPIE*, vol. 9772, no. 977205, February 2016.

[26] T. Kise, T. Suzuki, M. Funabashi, K. Nagashima, and H. Nasu, "The development of the 1060 nm 28 Gb/s VCSEL and the characteristics of the multi-mode fiber link," *Furukawa Review, Optical Communication*, vol. 46, pp. 7–12, March 2015.

[27] M.-J. Li, "MMF for high data rate and short length applications," *Optical Fiber Communication Conference (OFC)*, paper M3F.1, March 2014.

[28] L. Coldren and S. Corzine, *Diode lasers and photonic integrated circuits*, ser. Wiley series in microwave and optical engineering. New York, NY, USA: John Wiley & Sons, Inc., 1995.

[29] S. Adachi, "Lattice thermal resistivity of III-V compound alloys," *J. Applied Physics*, vol. 54, no. 4, pp. 1844–1848, 1983.

[30] P. Westbergh, J. S. Gustavsson, B. Kögel, Å. Haglund, and A. Larsson, "Impact of photon lifetime on high-speed VCSEL performance," *IEEE J. of Sel. Topics in Quantum Electronics*, vol. 17, no. 6, pp. 1603–1613, November-December 2011.

[31] E. P. Haglund, P. Westbergh, J. S. Gustavsson, and A. Larsson, "Impact of damping on high-speed large signal VCSEL dynamics," *IEEE J. of Lightwave Techn.*, vol. 33, no. 4, pp. 795–801, February 2015.

[32] K. Osamura and Y. Murakami, "Free carrier absorption in n-GaAs," *Japanese J. of Applied Physics*, vol. 11, no. 3, pp. 365–371, March 1972.

[33] W. Nakwaski and M. Osiński, "Thermal analysis of etched-well surface-emitting diode lasers," *Microwave and Optical Techn. Letters*, vol. 4, no. 12, pp. 541–543, November 1991.

[34] P. P. Baveja, B. Kögel, P. Westbergh, J. S. Gustavsson, Å. Haglund, D. N. Maywar, G. P. Agrawal, and A. Larsson, "Impact of device parameters on thermal performance of high-speed oxide-confined 850-nm VCSELs," *IEEE J. of Quantum Electronics*, vol. 48, no. 1, pp. 17–26, January 2012.

[35] B. Weigl, M. Grabherr, C. Jung, R. Jager, G. Reiner, R. Michalzik, D. Sowada, and K. J. Ebeling, "High-performance oxide-confined GaAs VCSELs," *IEEE J. of Sel. Topics in Quantum Electronics*, vol. 3, no. 2, pp. 409–415, April 1997.

[36] J. S. Gustavsson, Å. Haglund, J. Bengtsson, and A. Larsson, "High-speed digital modulation characteristics of oxide-confined vertical-cavity surface-emitting lasers - numerical simulations consistent with experimental results," *IEEE J. of Quantum Electronics*, vol. 38, no. 8, pp. 1089–1096, August 2002.

[37] R. S. Tucker, "High-speed modulation of semiconductor lasers," *IEEE Transactions on Electron Devices*, vol. 32, no. 12, pp. 2572–2584, December 1985.

[38] G. P. Agrawal, *Fiber-optic communications systems*, 3rd ed. New York, NY, USA: John Wiley & Sons, Inc., 2002, ch. 2, Optical fibers, pp. 38–50.

[39] P. Krehlik, "Directly modulated lasers in negative dispersion fiber links," *Opto-Electron. Review*, vol. 15, no. 2, pp. 71–77, June 2007.

[40] J. Lavrencik, S. K. Pavan, V. A. Thomas, and S. E. Ralph, "Noise in VCSEL-based links: Direct measurement of VCSEL transverse mode correlations and implications for MPN and RIN," *IEEE J. of Lightwave Techn.*, vol. 35, no. 4, pp. 698–705, February 2017.

[41] J. Lavrencik, J. S. Gustavsson, E. Haglund, A. Larsson, and S. E. Ralph, "Optimum VCSEL apertures for high-speed multimode fiber links," *Optical Fiber Communication Conference (OFC)*, paper M1I.1, March 2018.

[42] K. Ogawa, "Analysis of mode partition noise in laser transmission systems," *IEEE J. of Quantum Electronics*, vol. 18, no. 5, p. 849–855, May 1982.

[43] H. Li, P. Wolf, J. A. Lott, and D. Bimberg, "Relative intensity noise of temperature-stable, energy-efficient 980 nm VCSELs," *AIP Advances*, vol. 7, no. 2, pp. 025 107–1–025 107–5, February 2017.

[44] D. K. Serkland, G. A. Keeler, K. M. Geiba, and G. M. Peake, "Narrow linewidth VCSELs for high-resolution spectroscopy," *Proc. SPIE*, vol. 7229, no. 722907, pp. 1–8, February 2009.

[45] A. L. Schawlow and C. H. Townes, "Infrared and optical masers," *Physical Rev.*, vol. 112, no. 6, pp. 1940–1949, December 1958.

[46] C. H. Henry, "Theory of the linewidth of semiconductor lasers," *IEEE J. Quantum Electronics*, vol. 18, no. 2, pp. 259–264, February 1982.

[47] R. Nagarajan, M. Ishikawa, T. Fukushima, R. S. Geels, and J. E. Bowers, "High speed quantum-well lasers and carrier transport effects," *IEEE J. of Quantum Electronics*, vol. 28, no. 10, pp. 1990–2008, October 1992.

[48] P. Westbergh, R. Safaisini, E. Haglund, J. S. Gustavsson, A. Larsson, and A. Joel, "High-speed oxide confined 850-nm VCSELs operating error-free at 47 Gbit/s at room temperature and 40 Gbit/s at 85°C," *Conference on Lasers Electro-Optics Europe and International Quantum Electronics Conference (CLEO EUROPE/IQEC)*, paper CB-7.1, May 2013.

[49] E. Haglund, P. Westbergh, J. S. Gustavsson, E. P. Haglund, and A. Larsson, "High-speed VCSELs with strong confinement of optical fields and carriers," *IEEE J. of Lightwave Techn.*, vol. 34, no. 2, pp. 269–277, January 2016.

[50] S. B. Healy, E. P. O'Reilly, J. S. Gustavsson, P. Westbergh, Å. Haglund, A. Larsson, and A. Joel, "Active region design for high-speed 850-nm VCSELs," *IEEE J. of Quantum Electronics*, vol. 46, no. 4, pp. 506–512, April 2010.

[51] A. Mutig, G. Fiol, K. Potschke, P. Moser, D. Arsenijevic, V. A. Shchukin, N. Ledentsov, S. S. Mikhrin, I. L. Krestnikov, D. A. Livshits, A. Kovsh, F. Hopfer, and D. Bimberg, "Temperature-dependent small-signal analysis of high-speed high-temperature stable 980-nm VCSELs," *IEEE J. of Sel. Topics in Quantum Electronics*, vol. 15, pp. 679 – 686, July 2009.

[52] R. L. Naone, E. R. Hegblom, and L. A. Coldrenz, "Tapered-apertures for high-efficiency miniature VCSELs," *1999 digest of the LEOS summer topical meetings*, vol. 99TH8455, no. III, pp. 17–18, July 1999.

[53] J. M. Castro, R. Pimpinella, B. Kose, and B. Lane, "The interaction of modal and chromatic dispersion in VCSEL based multimode fiber channel links and its effect on mode partition noise," *International Wire & Cable Symposium (IWCS)*, no. 15-1, 2012.

[54] L. Raddatz, I. H. White, D. G. Cunningham, and M. C. Nowell, "Increasing the bandwidth-distance product of multimode fibre using offset launch," *Electronics Letters*, vol. 33, no. 3, pp. 232–233, January 1997.

[55] L. Raddatz, I. H. White, D. G. Cunningham and M. C. Nowell, "An experimental and theoretical study of the offset launch technique for the enhancement of the bandwidth of multimode fiber links," *IEEE J. of Lightwave Techn.*, vol. 16, no. 3, pp. 324–331, March 1998.

[56] R. Safaisini, K. Szczerba, E. Haglund, P. Westbergh, J. S. Gustavsson, A. Larsson, and P. A. Andrekson, "20 Gbit/s error-free operation of 850 nm oxide-confined VCSELs beyond 1 km of multimode fibre," *Electronics Letters*, vol. 48, no. 19, pp. 1225–1227, September 2012.

[57] R. Safaisini, K. Szczerba, P. Westbergh, E. Haglund, B. Kögel, J. S. Gustavsson, M. Karlsson, P. Andrekson, and A. Larsson, "High-speed 850nm quasi-single-mode VCSELs for extended-reach optical interconnects," *J. Opt. Commun. Netw.*, vol. 5, no. 7, pp. 686–695, July 2013.

[58] E. P. Haglund, Å. Haglund, P. Westbergh, J. S. Gustavsson, B. Kögel, and A. Larsson, "25 Gbit/s transmission over 500 m multimode fibre using 850 nm VCSEL with integrated mode filter," *Electronics Letters*, vol. 48, no. 9, pp. 517–519, April 2012.

[59] J. A. Tatum, D. Smith, J. K. Guenter, and R. H. Johnson, "Highspeed characteristics of VCSELs," *Proc. SPIE*, vol. 3004, May 1997.

[60] W. V. Sorin and M. R. Tan, "Interoperability of single-mode and multimode data links for data center and optical backplane applications," *Optical Fiber Communication Conference and Exposition and the National Fiber Optic Engineers Conference (OFC/NFOEC)*, paper OW1B.6, March 2013.

[61] Y. Satuby and M. Orenstein, "Mode-coupling effects on the small-signal modulation of multitransverse-mode vertical-cavity semiconductor lasers," *IEEE J. of Quantum Electronics*, vol. 35, no. 6, pp. 944–954, June 1999.

[62] J. S. Gustavsson, J. Bengtsson, and A. Larsson, "Modal dynamics and noise of vertical-cavity surface-emitting lasers," *International Conference*

on Numerical Simulation of Optoelectronic Devices (NUSOD), pp. 53–56, paper WD1, August 2004.

[63] J. S. Gustavsson, J. A. Vukusic, J. Bengtsson, and A. Larsson, "A comprehensive model for the modal dynamics of vertical-cavity surface-emitting lasers," *IEEE J. of Quantum Electronics*, vol. 38, no. 2, pp. 203–212, February 2002.

[64] R. Safaisini, E. Haglund, P. Westbergh, J. S. Gustavsson, and A. Larsson, "20 Gbit/s data transmission over 2 km multimode fibre using 850 nm mode filter VCSEL," *Electronics Letters*, vol. 50, no. 1, pp. 40–42, January 2014.

[65] J. M. Kahn and J. R. Barry, "Wireless infrared communications," *Proc IEEE*, vol. 85, no. 2, pp. 265–298, February 1997.

[66] N. Bamiedakis, A. Hashim, R. V. Penty, and I. H. White, "A 40 Gb/s optical bus for optical backplanel interconnections," *IEEE J. of Lightwave Techn.*, vol. 32, no. 8, pp. 1526–1537, April 2014.

[67] S. Walkin and J. Conradi, "Multilevel signaling for increasing the reach of 10 Gb/s lightwave systems," *IEEE J. of Lightwave Techn.*, vol. 17, no. 11, p. 2235–2248, November 1999.

[68] J. D. Ingham, R. V. Penty, and I. H. White, "10 Gb/s & 20 Gb/s extended-reach multimode-fiber data communication links using multilevel modulation and transmitter-based equalization," *Optical Fiber Communication Conference and Exposition and The National Fiber Optic Engineers Conference (OFC/NFOEC)*, paper OTuO7, February 2008.

[69] J. D. Ingham, R. V. Penty, I. H. White, P. Westbergh, J. S. Gustavsson, Å. Haglund, and A. Larsson, "32 Gb/s multilevel modulation of an 850 nm VCSEL for next-generation datacommunication standards," *Proc. CLEO*, paper CWJ2, May 2011.

[70] J. E. Cunningham, D. Beckman, X. Zheng, D. Huang, T. Sze, , and A. V. Krishnamoorthy, "PAM-4 signaling over VCSELs with 0.13 µm CMOS chip technology," *Optics Express*, vol. 14, no. 25, p. 12028–12038, December 2006.

[71] J. D. Ingham, R. V. Penty, and I. H. White, "10 Gb/s transmitter based equalization for extended-reach multimode-fiber data communication links," *Optical Fiber Communication Conference and Exposition and The National Fiber Optic Engineers Conference (OFC/NFOEC)*, paper OTuL4, March 2007.

[72] D. M. Kuchta, C. L. Schow, A. V. Rylyakov, J. E. Proesel, F. E. Doany, C. Baks, B. H. Hamel-Bissell, C. Kocot, L. Graham, R. Johnson, G. Landry, E. Shaw, A. MacInnes, and J. Tatum, "A 56.1 Gb/s NRZ modulated 850nm VCSEL-based optical link," *Optical Fiber Communication Conference (OFC)*, paper OW1B.5, June 2013.

[73] K. Maeda, T. Norimatsu, K. Kogo, N. Kohmu, K. Nishimura, and I. Fukasaku, "An active copper-cable supporting 56-Gbit/s PAM4 and 28-Gbit/s NRZ with continuous time linear equalizer IC for to-meters reach interconnection," *IEEE Symposium on VLSI Circuits*, June 2018.

[74] C. Xia, M. Ajgaonkar, and W. Rosenkranz, "On the performance of the electrical equalization technique in MMF links for 10-gigabit Ethernet," *IEEE J. of Lightwave Techn.*, vol. 23, no. 6, pp. 2001–2011, June 2005.

[75] R. Gitlin and S. Weinstein, "Fractionally-spaced equalization: An improved digital transversal equalizer," *Bell Syst. Tech. J.*, vol. 60, no. 2, pp. 275–296, February 1981.

[76] J. Gimlett and N. Cheung, "Dispersion penalty analysis for LED/single-mode fiber transmission systems," *IEEE J. of Lightwave Techn.*, vol. 4, no. 9, pp. 1381–1392, September 1986.

[77] F. Breyer, S. C. J. Lee, S. Randel, and N. Hani, "PAM-4 signalling for gigabit transmission over standard step-index plastic optical fibre using light emitting diodes," *European Conference on Optical Communication (ECOC)*, paper We.2.A.3, September 2008.

[78] I. Reed and G. Solomon, "Polynomial codes over certain finite fields," *J. Soc. Indust. Appl. Math.*, vol. 8, no. 2, pp. 300–304, June 1960.

[79] M. Freebody, "Lasers evolve to meet the demands of optical communications," *Photonics spectra*, vol. 46, pp. 50–53, February 2012.

[80] D. Mahgerefteh, C. Thompson, C. Cole, G. Denoyer, T. Nguyen, I. Lyubomirsky, C. Kocot, and J. Tatum, "Techno-economic comparison of silicon photonics and multimode VCSELs," *IEEE J. of Lightwave Techn.*, vol. 34, no. 2, pp. 233–242, January 2016.

[81] L. Qiu, E. J. Lawrence, B. Ayres, M. Schumacher, A. Amezcua, D. Molin, and G. Kuyt, "40GBASE-SR4 frame error rate test of chromatic dispersion compensating MMF," *Optical Fiber Communication Conference and Exposition and the National Fiber Optic Engineers Conference (OFC/NFOEC)*, paper NW1J.6, March 2013.

[82] T. N. Huynh, F. Doany, D. M. Kuchta, D. Gazula, E. Shaw, J. O'Daniel, and J. Tatum, "4 x 50Gb/s NRZ shortwave-wavelength division multiplexing VCSEL link over 50m multimode fiber," *Optical Fiber Communications Conference and Exhibition (OFC)*, paper Tu2B.5, March 2017.

[83] J. M. Castro, R. Pimpinella, B. Kose, P. Huang, B. Lane, K. Szczerba, P. Westbergh, T. Lengyel, J. S. Gustavsson, A. Larsson, and P. A. Andrekson, "Investigation of 60 Gb/s 4-PAM using an 850 nm VCSEL and multimode fiber," *IEEE J. of Lightwave Techn.*, vol. 34, no. 16, pp. 3825–3836, August 2016.

[84] G. Stepniak, J. R. Kropp, N. N. Ledentsov, V. A. Shchukin, N. Ledentsov, G. Schaefer, and J. P. Turkiewicz, "54 Gbps OOK transmission using single mode VCSEL up to 1 km OM4 MMF," *Optical Fiber Communications Conference and Exhibition (OFC)*, paper Th4D.5, March 2016.

[85] I. C. Lu, C. C. Wei, H. Y. Chen, K. Z. Chen, C. H. Huang, K. L. Chi, J. W. Shi, F. I. Lai, D. H. Hsieh, H. C. Kuo, W. Lin, S. W. Chiu, and J. Chen, "Very high bit-rate distance product using high-power single-mode 850-nm VCSEL with discrete multitone modulation formats through OM4 multimode fiber," *IEEE J. of Sel. Topics in Quantum Electronics*, vol. 21, no. 6, pp. 444–452, November 2015.

[86] C. Kottke, C. Caspar, V. Jungnickel, R. Freund, M. Agustin, and N. N. Ledentsov, "High speed 160 Gb/s DMT VCSEL transmission using pre-equalization," *Optical Fiber Communications Conference and Exhibition (OFC)*, paper W4I.7, March 2017.

[87] D. Kuchta, A. V. Rylyakov, C. L. Schow, J. Proesel, C. Baks, P. Westbergh, J. S. Gustavsson, and A. Larsson, "64Gb/s transmission over 57m MMF using an NRZ modulated 850nm VCSEL," *Optical Fiber Communication Conference (OFC)*, paper Th3C.2, March 2014.

[88] J. J. Liu, K. L. Chi, C. C. Wei, T. C. Lin, C. Y. Chuang, X. N. Chen, J. W. Shi, and J. Chen, "High bit-rate distance product of 128 Gbps.km 4-PAM transmission over 2-km OM4 fiber using an 850-nm VCSEL and a Volterra nonlinear equalizer," *Optical Fiber Communications Conference and Exhibition (OFC)*, paper W3G.5, March 2017.

[89] T. Zuo, L. Zhang, J. Zhou, Q. Zhang, E. Zhou, and G. N. Liu, "Single lane 150-Gb/s, 100-Gb/s and 70-Gb/s 4-PAM transmission over 100-m, 300-m and 500-m MMF using 25-G class 850nm VCSEL," *European Conference on Optical Communication (ECOC)*, paper Th.1.C.2, September 2016.

[90] F. Chang, Y. Sun, R. Lingle, Y. Zhang, P. Cai, M. Huang, D. Pan, T. Gray, S. Bhoja, S. Nelson, and J. Tatum, "First demonstration of PAM4 transmissions for record reach and high-capacity SWDM links over MMF using 40G/100G PAM4 IC chipset with real-time DSP," *Optical Fiber Communications Conference and Exhibition (OFC)*, paper Tu2B.2, March 2017.

[91] J. Lavrencik, S. Varughese, V. A. Thomas, G. Landry, Y. Sun, R. Shubochkin, K. Balemarthy, J. Tatum, and S. E. Ralph, "4λ x 100Gbps VCSEL PAM-4 transmission over 105m of wide band multimode fiber," *Optical Fiber Communication Conference (OFC)*, paper Tu2B.6, March 2017.

[92] Y. Sun, J. Kamino, R. Shubochkin, A. Swartz, R. Lingle, and D. Braganza, "High speed short reach optical interconnect over OM4 and OM5 multimode optical fiber," *International Wire & Cable Symposium (IWCS)*, no. 18-6, pp. 791–796, October 2017.

[93] N. Suzuki, H. Hatakeyama, K. Fukatsu, T. Anan, K. Yashiki, and M. Tsuji, "25 Gbit/s operation of InGaAs-based VCSELs," *Electronics Letters*, vol. 42, no. 17, pp. 975–976, August 2006.

[94] K. Yashiki, N. Suzuki, K. Fukatsu, T. Anan, H. Hatakeyama, and M. Tsuji, "1.1-µm-range high-speed tunnel junction vertical-cavity surface-emitting lasers," *IEEE Photonics Techn. Letters*, vol. 19, no. 23, pp. 1883–1885, December 2007.

[95] N. Suzuki, T. Anan, H. Hatakeyama, K. Fukatsu, K. Yashiki, K. Tokutome, T. Akagawa, and M. Tsuji, "High speed 1.1-µm-range InGaAs-based VCSELs," *IEICE Trans. on Electronics*, vol. E92.C, no. 7, pp. 942–950, July 2009.

[96] Y. Zheng, C. H. Lin, A. V. Barve, and L. A. Coldren, "p-type δ-doping of highly-strained VCSELs for 25 Gbps operation," *IEEE Photonics Conference (IPC)*, pp. 131–132, paper MP3, September 2012.

[97] A. Tatarczak, Y. Zheng, G. A. Rodes, J. Estaran, C. H. Lin, A. V. Barve, R. Honoré, N. Larsen, L. A. Coldren, and I. T. Monroy, "30 Gbps bottom-emitting 1060 nm VCSEL," *European Conference on Optical Communication (ECOC)*, paper P.2.3, September 2014.

[98] T. Suzuki, M. Funabashi, H. Shimizu, K. Nagashima, S. Kamiya, and A. Kasukawa, "1060nm 28-Gbps VCSEL developed at Furukawa," *Proc. SPIE*, vol. 9001, no. 900104, January 2014.

[99] J. B. Héroux, T. Kise, M. Funabashi, T. Aoki, C. L. Schow, A. V. Rylyakov, and S. Nakagawa, "Energy-efficient 1060-nm optical link operating up to 28 Gb/s," *IEEE J. of Lightwave Techn.*, vol. 33, no. 4, pp. 733–740, February 2015.

[100] K. Nagashima, T. Kise, Y. Ishikawa, and H. Nasu, "A record 1-km MMF NRZ 25.78-Gb/s error-free link using a 1060-nm DIC VCSEL," *IEEE Photon. Techn. Letters*, vol. 28, no. 4, pp. 418–420, February 2016.

[101] S. K. Pavan, J. Lavrencik, R. Shubochkin, Y. Sun, J. Kim, D. Vaidya, R. Lingle, T. Kise, and S. E. Ralph, "50Gbit/s PAM-4 MMF transmission using 1060nm VCSELs with reach beyond 200m," *Optical Fiber Communication Conference and Exposition (OFC)*, paper W1F.5, March 2014.

[102] M. Tan, P. Rosenberg, W. Sorin, S. Mathai, G. Panotopoulos, G. Rankin, and J. Straznicky, "Progress towards low cost Tbps optical engines," *IEEE CPMT Symposium Japan (ICSJ)*, pp. 9–11, November 2015.

[103] M. R. Tan, P. Rosenberg, W. V. Sorin, S. Mathai, G. Panotopoulos, and G. Rankin, "Universal photonic interconnect for data centers," *Optical Fiber Comm. Conference (OFC)*, paper Tu2B.4, March 2017.

[104] R. Rosales, M. Zorn, and J. A. Lott, "30-Ghz small-signal modulation bandwidth with directly current-modulated 980-nm oxide-aperture VCSELs," *IEEE Photon. Techn. Letters*, pp. 533–534, October 2017.

[105] G. Larisch, P. Moser, J. A. Lott, and D. Bimberg, "Large bandwidth, small current density, and temperature stable 980-nm VCSELs," *IEEE J. of Quantum Electronics*, vol. 53, no. 6, pp. 1–8, December 2017.

[106] A. Malacarne, V. Sorianello, A. Daly, B. Kögel, M. Ortsiefer, S. Melo, C. Neumeyr, M. Romagnoli, and A. Bogoni, "High speed long wavelength VCSELs for energy efficient 40 Gbps links up to 1 km without error correction," *Optical Fiber Communication Conference (OFC)*, paper Tu2H.1, March 2015.

[107] M. Müller, P. W. andTobias Gründl, C. Grasse, J. Rosskopf, W. Hofmann, D. Bimberg, and M.-C. Amann, "Energy efficient 1.3 µm short cavity VCSELs for 30 Gb/s error-free optical links," *IEEE International Semiconductor Laser Conference (ISLC)*, paper PD2, October 2012.

[108] D. Kuchta, F. E. Doany, L. Schares, C. Neumeyr, A. Daly, B. Kögel, J. Rosskopf, and M. Ortsiefer, "Error-free 56 Gb/s NRZ modulation of a 1530 nm VCSEL link," *European Conference on Optical Communication (ECOC)*, paper PDP.1.3, December 2015.

[109] E. P. Haglund, P. Westbergh, J. S. Gustavsson, E. P. Haglund, A. Larsson, M. Geen, and A. Joel, "30 Ghz bandwidth 850 nm VCSEL with sub-100 fJ/bit energy dissipation at 25-50 Gbit/s," *Electronics Letters*, vol. 51, no. 14, pp. 1096–1098, July 2015.

[110] P. Westbergh, E. P. Haglund, E. Haglund, R. Safaisin, J. S. Gustavsson, and A. Larsson, "High speed 850 nm VCSELs operating error-free up to 57 Gbit/s," *Electronics Letters*, vol. 49, no. 16, pp. 1021–1023, August 2013.

[111] E. Haglund, M. Jahed, J. S. Gustavsson, A. Larsson, J. Goyvaerts, R. Baets, G. Roelkens, M. Rensing, and P. O'Brien, "High-power single transverse and polarization mode VCSEL for silicon photonics integration," *Optics Express*, vol. 19, no. 13, pp. 18 892–18 899, January 2019.